Phytochemistry 147 (2018) 30–48

Contents lists available at ScienceDirect

Phytochemistry

journal homepage: www.elsevier.com/locate/phytochem

Potato native and wound periderms are differently affected by down-regulation of FHT, a suberin feruloyl transferase

Liqing Jin [a, b, 1], Qing Cai [a, c, 1], Wenlin Huang [a], Keyvan Dastmalchi [a], Joan Rigau [d], Marisa Molinas [e], Mercè Figueras [e], Olga Serra [e], Ruth E. Stark [a, b, c, *]

[a] Department of Chemistry and Biochemistry, The City College of New York, City University of New York and CUNY Institute for Macromolecular Assemblies, New York, NY 10031, USA
[b] Program in Biochemistry, The Graduate Center of the City University of New York, New York, NY 10016, USA
[c] Program in Chemistry, The Graduate Center of the City University of New York, New York, NY 10016, USA
[d] Centre for Research in Agricultural Genomics, Consorci CSIC-IRTA-UAB-UB, Campus de Bellaterra UAB, E-08193, Cerdanyola Del Vallès, Barcelona, Spain
[e] Laboratori Del Suro, Departament de Biologia, University of Girona, Campus Montilivi, Girona, E-17071 Spain

ARTICLE INFO

Article history:
Received 11 August 2017
Received in revised form
11 December 2017
Accepted 14 December 2017
Available online 27 December 2017

Keywords:
GC-MS
FHT: suberin feruloyl transferase
LC-MS
Periderm suberin and wax
Phellem
Solanum tuberosum
Potato skin
Solid-state NMR
Thioacidolysis

ABSTRACT

Potato native and wound healing periderms contain an external multilayered phellem tissue (potato skin) consisting of dead cells whose cell walls are impregnated with suberin polymers. The phellem provides physical and chemical barriers to tuber dehydration, heat transfer, and pathogenic infection. Previous RNAi-mediated gene silencing studies in native periderm have demonstrated a role for a feruloyl transferase (FHT) in suberin biosynthesis and revealed how its down-regulation affects both chemical composition and physiology. To complement these prior analyses and to investigate the impact of FHT deficiency in wound periderms, a bottom-up methodology has been used to analyze soluble tissue extracts and solid polymers concurrently. Multivariate statistical analysis of LC-MS and GC-MS data, augmented by solid-state NMR and thioacidolysis, yields two types of new insights: the chemical compounds responsible for contrasting metabolic profiles of native and wound periderms, and the impact of FHT deficiency in each of these plant tissues. In the current report, we confirm a role for FHT in developing wound periderm and highlight its distinctive features as compared to the corresponding native potato periderm.

1. Introduction

Potato (*Solanum tuberosum* L.) ranks as the fifth largest staple crop consumed worldwide, fulfilling essential needs in human nutrition and health (FAO, 2015). The complex dermal structure or periderm that covers plant tubers is critical to the quality, storage, and shelf life of potatoes. Its outermost layer, designated as the phellem, consists of several strata of dead cells with suberized walls. The phellem forms the potato cork skin and provides the first line of constitutive defense for the tuber against dehydration, heat transfer, and pathogen infection, including both physical and chemical barriers. The chemical barrier consists of soluble phenolic compounds such as hydroxycinnamic acids and their amide derivatives, flavonoids, and glycoalkaloids, some of which display beneficial antioxidant properties (Akyol et al., 2016). The physical barrier comprises the phellem cellulose cell wall in which the complex polyaliphatic and polyphenolic (lignin-like) suberin materials are deposited (Bernards, 2002).

Suberin is a fatty polyester that upon transesterification releases mainly soluble C_{16}–C_{28} ω-hydroxyacids and α,ω-dicarboxylic acids as well as fatty acids (alkanoic acids), primary alcohols (1-alkanols), glycerol, and very small amounts of ferulic acid (Graça and Santos, 2007). It is deposited at the internal side of the cell wall facing the plasma membrane, forming an insoluble matrix within which are embedded a complex mixture of extractable lipids, collectively

Abbreviations: **4CL**, 4-Hydroxycinnamic acid; **PHT**, Putrescine hydroxycinnamoyltransferase; **FHT**, Fatty ω-hydroxyacid/fatty alcohol hydroxycinnamoyltransferase; **THT**, Tyramine N-Hydroxycinnamoyltransferase; **CYP**, Cytochrome P450 monooxygenase; **FAR**, Alcohol-forming fatty acyl-CoA reductase; **G3P**, Glycerol-3-phosphate; **GPAT**, Glycerol 3-phosphate acyltransferase. * saturated and unsaturated carbon chains.

* Corresponding author. 160 Convent Avenue, New York, NY 10031.
E-mail address: rstark@ccny.cuny.edu (R.E. Stark).

[1] These two authors contributed equally to this work.

https://doi.org/10.1016/j.phytochem.2017.12.011
0031-9422/

called wax and substantially similar to the released suberin monomers found in potato (Schreiber et al., 2005). The more recalcitrant lignin-like portion of the polymeric material, composed principally of *p*-hydroxycinnamates (e.g., ferulate, *p*-coumarate, and sinapate) and their derivatives, is deposited within the polysaccharide primary cell wall (Lapierre et al., 1995). The aliphatic and the phenolic polymeric structures are spatially separated (Yan and Stark, 1998; Gil et al., 1997), but they have been proposed to be linked covalently through ferulate ester bonds (Graça and Santos, 2007).

When the potato skin is broken, the tuber reacts rapidly to restore the barriers by forming a new periderm (wound periderm) that achieves impermeability and chemical defense for the newly exposed fleshy tissues. The healing process proceeds in two stages (Sabba and Lulai, 2002). First, cells adjacent to the wound surface exhibit an increase in polyamines and deposit suberin polymers prior to cell death, forming a wound closing layer within 1–3 days post-wounding. Secondly, a new periderm is formed internally by cell division during the next 5–12 days, where the time course is modulated by the environmental and physiological conditions under which the healing process takes place (Dean and Kolattukudy, 1976; Lulai and Corsini, 1998). Native and wound periderms have similar anatomical structures and undergo analogous maturation processes until they acquire resistance to excoriation (Sabba and Lulai, 2002). However, comparing mature wound and native periderms, the wound periderm is two orders of magnitude more permeable to water. At 21 days post-wounding, its released suberin and wax content is only 50–60% that of native periderm, but its wax fraction is proportionally enriched in alkyl ferulates (Schreiber et al., 2005). Comparison of native mature periderm and 7-day immature wound periderms by solid-state ^{13}C nuclear magnetic resonance (ssNMR) reveals that at this early-stage wound periderm has an enhanced hydrophilic–hydrophobic balance, lignin-like polymeric structures that are more resistant to degradation, and more flexible aliphatic chains, suggestive of a remodeled supramolecular organization (Serra et al., 2014). Achieving a better metabolic understanding of the wound compared with native periderm has the potential to improve the outcomes of crop management.

A fatty ω-hydroxyacid/fatty alcohol hydroxycinnamoyl transferase), FHT, is the enzyme responsible for the formation of alkyl ferulates in potato periderm, whereby fatty ω-hydroxyacids and fatty alcohols are esterified to feruloyl moieties (Serra et al., 2010). Down-regulation of ferulate ester synthesis by *FHT*-RNAi silencing leads to a reduction in alkyl ferulates in both the hydrolyzable aliphatic suberin and the extractable wax from native periderms (Graça, 2015; Serra et al., 2010). That is, native FHT-deficient periderms yield much lower quantities of ferulic acid (72% reduction), C18:1 ω-hydroxyacids (76% reduction), and most primary alcohols by suberin transesterification compared with wild-type (WT) native skins. However, because FHT-deficient tubers experience a concomitant increase in the periderm thickness, the total amount of hydrolyzable suberin, measured as μg-cm^{-2}, remains virtually unchanged. As regards the embedded wax fraction, ferulate and alkanes are greatly reduced (72% and 70%, respectively), but the overall amount of wax compounds is doubled due mainly to increases in fatty acids and 1-alkanols. Moreover in *FHT*-RNAi native tubers, transpiration via the tuber skin is enhanced 14-fold and the skin takes on a very russeted and brittle appearance, but notably, the typical lamellated ultrastructure of the cell wall remains intact (Serra et al., 2010). Furthermore, the macromolecular organization and mechanical properties of the *FHT*-RNAi native periderm are compromised. Solid-state ^{13}C NMR analysis reveals abundant aromatic constituents that resist transesterification whereas the aliphatic chains exhibit changes in flexibility that can be linked to both resistance to deformation and mechanical resiliency (Serra et al., 2014). On the other hand, although an intriguing activation of the *FHT* promoter has been observed in WT wounded periderm (Boher et al., 2013; Lulai and Neubauer, 2014), it is not yet known how FHT deficiency impacts the chemical composition or supramolecular organization of the wound tissues.

To gain a deeper understanding of native and wound periderms and to investigate the impact of FHT in healing tissue, the current work compares these two tissue types from *FHT*-RNAi and WT tubers in parallel using immature periderms from freshly-harvested tubers and healing disks. A bottom-up metabolomic approach, combining metabolite profiling with ssNMR, is used to compare the soluble metabolites and the insoluble cell-wall embedded structural moieties of the respective native and wound periderms. To add molecular insights for the lignin-like polymeric materials in suberized cell walls, the soluble phenolics obtained from a degradative thioacidolysis treatment are also compared. This 'holistic' analysis of native and wound-healing periderm both complements and augments the earlier investigations, yielding comprehensive and statistically robust information about the impact of knocking down the *FHT* gene in these protective plant tissues.

2. Results

Parenchyma-free phellem tissues, isolated by skinning freshly-harvested tubers and the wound tuber disks, were first extracted to obtain polar and non-polar soluble metabolites. The insoluble interfacial residue was then treated enzymatically to remove any unsuberized cell walls and remaining waxes before ssNMR analysis, as described in the Materials and Methods section. The following overview of our investigative strategy lays the groundwork for the specific findings presented in the subsequent sections.

Native and wound periderms contain diverse soluble metabolites of differing polarity, chemical class, and abundance. In this context, a broadly applicable biphasic extraction approach was used to concurrently separate the samples into soluble polar and non-polar extracts plus an insoluble solid suspension (Choi et al., 2004; Kim et al., 2010; Wolfram, 2006). For the soluble metabolites, multivariate statistics were used to conduct Principal Component Analysis (PCA) of liquid chromatography – mass spectrometry (LC-MS) and gas chromatography (GC-MS) data for the respective types of extracts. Then, to identify those metabolites that were unique or had notably increased or decreased relative abundance in a particular sample (potential biomarkers), an Orthogonal Partial Least Squares Discriminant Analysis (OPLS-DA (Worley and Powers, 2013),) was performed. By displaying the covariance and correlation from the OPLS-DA model as a scatter plot (S-plot), we visualized both the magnitude of the enhanced abundance (P [1]) and the reliability of the effect (P (corr)[1]). Points in the S-plot 'wings' were then linked to the corresponding chromatographic retention times, *m/z* values, and particular chemical compounds by comparison with reference databases or published MS data including molecular ions and fragmentation patterns (Wiklund, 2008). The insoluble solid suspension containing the interfacial residue was analyzed to deduce types and relative numbers of the major carbon-containing moieties by high-resolution ^{13}C ssNMR as well as examination of the ether-linked polyphenolic thioacidolysis breakdown products. First, we compared *FHT*-RNAi with WT for native and wound periderms (14 days post-wounding) with respect to their polar and non-polar soluble metabolites and the corresponding interfacial residues. Then, we compared native with wound periderm in each of the WT and *FHT*-RNAi tubers. Finally, to better understand the formation of the wound periderm, we analyzed extracts and solid suspensions

from three other key points of the healing process (0 days, 3 days, and 7 days post-wounding), together with the wound periderm (14 days post-wounding), for both WT and *FHT*-RNAi issues.

2.1. FHT-RNAi vs WT native and wound periderm

2.1.1. The soluble polar extracts

Polar extracts from *FHT*-RNAi and WT native periderms were analyzed by LC-MS. In Fig. 1A, the score plot illustrates that the polar metabolites detected by negative-mode LC-MS (*m/z* 100–1300) from nine replicates each of *FHT*-RNAi and WT samples cluster very well but are clearly separated from each other with respect to the first principal component, indicating notable and consistent changes associated with *FHT* silencing. Fig. S1 (top) represents superimposed chromatograms from nine biological replicates each of WT and *FHT*-RNAi, which show excellent reproducibility and reveal clear differences in metabolite abundance between WT and *FHT*-RNAi, as expected from the PCA analysis. Analogous discrimination is observed in positive-mode LC-MS data from polar extracts (Fig. S2) and in NMR-based PCA score plots (Fig. S3, top). Using OPLS-DA (Fig. 2) and drawing on prior MS reports, we identified 25 of 33 differentially accumulated metabolites (potential biomarkers) that belong to various structural classes and discriminate between the *FHT*-RNAi and WT soluble polar extracts. Those compounds present at elevated abundance in *FHT*-RNAi extracts included phenolic amines such as feruloyltyramine (FT), feruloylputrescine (FP), caffeoylputrescine (CafP), and amide dimers such as dihydrocaffeoylputrescine (DHCafP), two grossamide (FT + FT) isomers, and dimers derived from feruloyloctopamine (FO-FO), dihydro-FT-FO, and FT-FO (Table 1). Conversely, phenolic acids related to caffeoyl quinic acid and glycoalkaloids such as α-chaconine, α-solanine, and protodioscin were highly abundant in WT (Table 1) (Dastmalchi et al., 2014; Dawid and Hofmann, 2014; Duo et al., 2007; Matsuda et al., 2005; Narvaez-Cuenca et al., 2012; Shakya and Navarre, 2008). To put these findings into context, all 35 polar identified metabolites are listed in Table S1.

The soluble polar extracts were also analyzed in day-14 wound periderms. However, no significant differences between *FHT*-RNAi and WT could be detected by PCA analysis and no differentially accumulated metabolites could be identified (data presented below with the wound-healing time course).

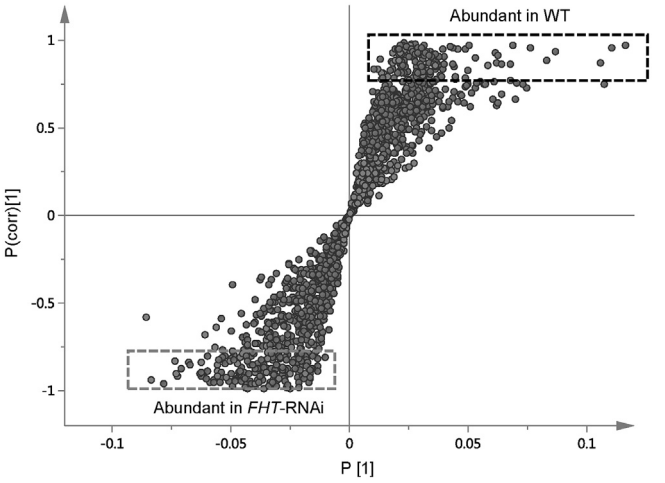

Fig. 2. Scatter plot (S-plot) highlighting compounds that contribute significantly to differing metabolite profiles for the wild-type (WT) and *FHT*-RNAi silenced native potato periderms derived from negative-mode LC-MS of their polar extracts. P [1] shows the magnitude of enhanced relative abundance for each metabolite, and P (corr) [1] indicates the reliability of the effect. MS ions at the extreme 'wings' of the plot (P (corr)[1] values greater than 0.80) were designated as potential biomarkers and checked for specificity to the cultivar type using a variable line plot (Fig. S4).

2.1.2. The soluble non-polar extracts

Non-polar extracts were analyzed by GC-MS (*m/z* 45–600) and compared. The score plot in Fig. 1B and chromatograms in Fig. S1 (bottom) illustrate that the soluble non-polar metabolites detected by GC-MS from nine replicates of each *FHT*-RNAi and WT sample cluster very well, respectively. As observed for the corresponding polar extracts (Fig. 1, left), the non-polar extracts are clearly separated from each other with respect to the first principal component, indicating notable and consistent changes associated with *FHT* silencing. Analogous discrimination was found for the NMR-based PCA score plot (Fig. S3, bottom). Twenty-five of the 31 metabolites accumulated differentially by *FHT*-RNAi and WT could

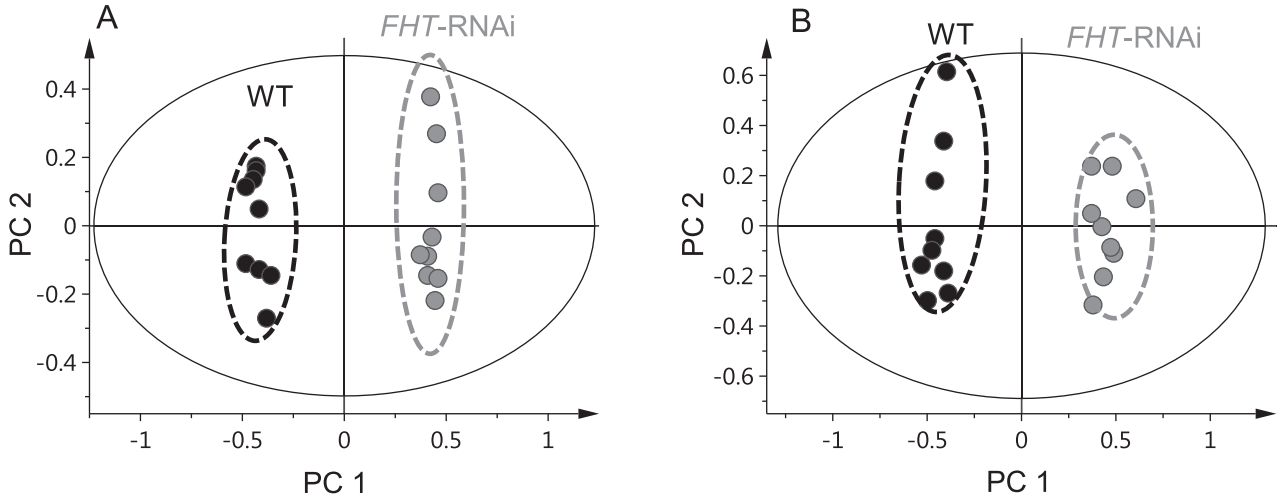

Fig. 1. PCA score plots for metabolomic analysis of soluble extracts from native potato periderms, with 9 biological replicate clusters color-coded for WT (black) and *FHT*-RNAi (gray) potato periderms. A: Polar extracts examined by negative-mode LC-MS. B: Non-polar extracts examined by GC-MS. Data were analyzed using SIMCA-P^{+} software; the x and y axes represent the score values of principal components 1 and 2, respectively.

Table 1
Differentially Accumulated metabolites between *FHT*-RNAi and WT by chemical class and structure for polar extracts from native potato periderms.

No.	Ions [a]	TOF [b] (error)	MS/MS Fragment ion[a]	Compound Name, Formula	Molecular Structure	Ref.
Highly Abundant *FHT*-RNAi Metabolites						
Phenolic amines						
1	250.9 $[M-H]^-$	251.1399 (0.8 ppm)	129.0, 120.9, 93.0	dihydro-Caffeoylputrescine $C_{13}H_{20}N_2O_3$	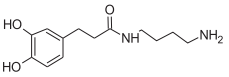	Not reported
2	249.3[c] $[M-H]^-$	249.1255 (4.4 ppm)	207.1, 160.9, 148.1, 135, 107.1	Caffeoylputrescine $C_{13}H_{18}N_2O_3$	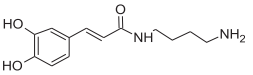	(Matsuda et al., 2005; Dastmalchi et al., 2014)
3	265.1[d] $[M+H]^+$	265.1536 (-3.8 ppm)	248.1, 177.0, 145.0	Feruloylputrescine $C_{14}H_{20}N_2O_3$	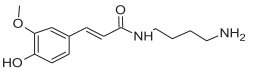	(Matsuda et al., 2005; Dastmalchi et al., 2014)
4	312.1[c] $[M-H]^-$	312.1236 (0.9 ppm)	297.1, 190.2, 178.8, 148.1	N-Feruloyltyamine (FT) $C_{18}H_{19}NO_4$	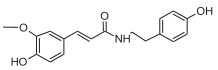	(Matsuda et al., 2005; Dastmalchi et al., 2014)
5	623.4 $[M-H]^-$	623.2405 (1.0 ppm)	460.2, 445.4, 336.2, 324.2, 322.2	Grossamide (FT-FT dimer) $C_{36}H_{36}N_2O_8$	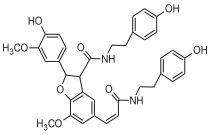	(Serra et al., 2010; Dastmalchi et al., 2014)
6	623.3 $[M-H]^-$	623.2405 (1.0 ppm)	460.2, 444.2, 623.4, 283.1, 336.1, 445.2	Grossamide (FT-FT dimer) $C_{36}H_{36}N_2O_8$	*Cis/trans* Grossamide	
7	655.3 $[M-H]^-$	655.2301 (0.6 ppm)	655.3, 637.3, 619.4, 484.3, 476.3, 458.3, 415.4, 297.3	FO-FO dimer $C_{36}H_{36}N_2O_{10}$	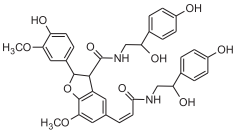	Not reported
8	641.4 $[M-H]^-$	641.2513 (-1.0 ppm)	623.4, 489.2, 460.2, 336.2, 326.2, 312.2, 151.0	Dihydro-FT-FO dimer $C_{36}H_{38}N_2O_9$	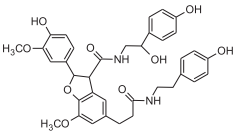	Not reported
9	639.4 $[M-H]^-$	639.2346 (0.6 ppm)	621.5, 460.4, 297.3, 578.5, 486.3, 458.3, 415.4	FT-FO dimer $C_{36}H_{36}N_2O_9$	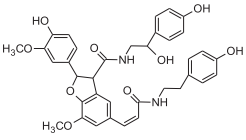	(King and Calhoun, 2010; Serra et al., 2010; Landgraf et al., 2014)
Incompletely Identified Constituents						
10	721.2	721.1606	721.2, 706.3, 585.4, 570.3, 555.4, 529.3, 512.3, 407.3, 391.3, 348.2, 191,150	phenolic amines		
11	803.2	803.3113	803.3, 641.3, 623.3, 489.3, 326.2, 312.2, 151.1	cinnamic acid derivative		
12	602.3		602.2, 341.2, 328.2, 282.1, 250.1, 245.0, 231.0, 193.0, 151.0, 136.0			
Highly Abundant WT Metabolites						
Phenolic acids						
13	353.1[c] $[M-H]^-$	353.0870 (-0.8 ppm)	191.0, 161.1, 135	caffeoyl quinic acid isomer $C_{16}H_{18}O_9$	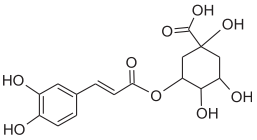	(Narvaez-Cuenca et al., 2012; Dastmalchi et al., 2014)
14	375.0 $[M + Na-H]^-$	375.0701 (0.8 ppm)	201.0, 179.0, 161.1, 135	$C_{16}H_{17}O_9Na$		
15	353.1 $[M-H]^-$	353.0870 (-0.8 ppm)	191.0, 161.1, 135	caffeoyl quinic acid isomer $C_{16}H_{18}O_9$		
16	375.8 $[M + Na-H]^-$	375.0701 (0.8 ppm)	201.0, 179.0, 161.1, 135	$C_{16}H_{17}O_9Na$		
17	179.1 $[M-H]^-$		161, 135.0, 107.0, 89	Caffeic acid $C_9H_8O_4$	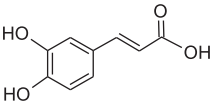	(Narvaez-Cuenca et al., 2012)

(*continued on next page*)

Table 1 (*continued*)

No.	Ions [a]	TOF [b] (error)	MS/MS Fragment ion[a]	Compound Name, Formula	Molecular Structure	Ref.
Glycoalkaloids						
18	866.2[c] [M-H]$^-$	866.4918 (1.2 ppm)	720.5, 704.5, 558.5	α-Solanine $C_{45}H_{73}NO_{15}$	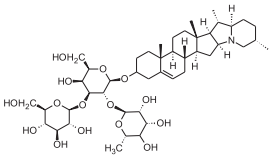	(Matsuda et al., 2005; Shakya and Navarre, 2006; Dastmalchi et al., 2014)
19	912.5[c] [M + HCOOH−H]$^-$	912.4982 (2.3 ppm)	866.5, 720.6, 704.5	α-Solanine + HCOOH $C_{45}H_{73}NO_{15}$.HCOOH		
20	850.1[c] [M-H]$^-$	850.4993 (4.1 ppm)		α-Chaconine $C_{45}H_{73}NO_{14}$	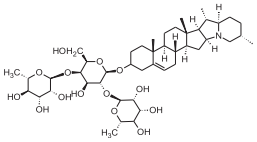	(Matsuda et al., 2005; Shakya and Navarre, 2006; Dastmalchi et al., 2014)
21	896.5[c] [M + HCOOH−H]$^-$	896.5046 (3.8 ppm)	850.5, 704.5	α-Chaconine + HCOOH $C_{45}H_{73}NO_{14}$.HCOOH		
22	704.3 [M-H]$^-$	704.4374 (0.7 ppm)	558.6, 112.9	Solanidine-Glc-Rha $C_{39}H_{63}NO_{10}$	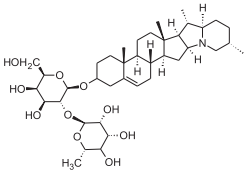	(Matsuda et al., 2005)
23,24	1049.8[c] [M-H]$^-$ 1095.7[c] [M + HCOOH−H]$^-$	1049.5568 (2.9 ppm)	903.4, 757.4, 741.4, 433.4	Dihydro-ASP-II $C_{51}H_{86}O_{22}$	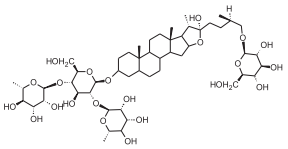	(Dawid and Hofmann, 2014)
25	1061.8	1061.5220 (4.3 ppm)	915.4, 899.4, 881.4, 753.5, 735.5, 687.4, 573.5, 555.5	$C_{51}H_{84}O_{23}$	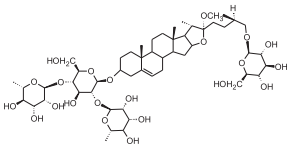	Not reported
26,27	1047.7 [M-H]$^-$ 1093.7 [M + HCOOH−H]$^-$	1047.5391 (0.9 ppm)	901.5, 883.5, 755.4, 737.5	Protodioscin /neoprotodioscin $C_{51}H_{84}O_{22}$	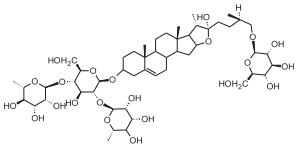	(Dawid and Hofmann, 2014)
Other Constituents						
28	191.1 [M-H]$^-$	191.0557 (2.1 ppm)	147.0, 111.0, 87.0	Quinic acid $C_7H_{12}O_6$	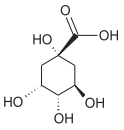	(Duo et al., 2007)
Incompletely Identified Constituents						
29	1045.7	1045.5243 (1.7 ppm)	1027.4899.4, 881.4, 735.4, 555.4	$C_{51}H_{82}O_{22}$		
30	933.5 [M-H]$^-$	933.2677 (-0.7 ppm)	753.2, 771.3, 449.1, 287.1	$C_{43}H_{50}O_{23}$ Flavonoid		
31	925.0	925.4343	717.4, 570.4, 553.1, 511.4			
32	1063.6	1063.5422 (25 ppm)	1045, 903, 883.5, 721.4			
33	1033.7 [M-H]$^-$ 1079.7 [M + HCOOH−H]$^-$	1033.5624 (3.4 ppm)	887.5, 869.5, 741.5, 723.5	$C_{51}H_{86}O_{21}$	1049-O	

[a] Ions and fragmentation data obtained from LC-MS and LC-MS^2 analysis using a 4000Q Trap instrument.
[b] Exact mass data obtained from TOF data analysis.
[c] Metabolites that distinguish polar extracts from native periderms of four cultivars (Atlantic, Chipeta, Norkotah Russet, Yukon Gold) (Huang et al., 2017).
[d] Positive-mode LC-MS.

be selected by OPLS-DA (Fig. S4) as outlined above and then identified (Table 2) (Dastmalchi et al., 2015; Graça and Pereira 2000; Huang et al., 2017; Serra et al., 2010; Yang and Bernards, 2007). In *FHT*-RNAi the highly abundant metabolites included long-chain saturated fatty acids (C22, C23, C24, C27), long-chain primary alcohols (C22, C26, C27, C28, C29), methyl esters (C17:0, C19:2), 1-monohexadecanoyl glycerol and glucose. In WT the highly abundant metabolites included alkanes (C21, C23, C25, C27, C29),

Table 2
Differentially Accumulated metabolites between *FHT*-RNAi and WT by chemical class and structure for non-polar extracts from native potato periderms.

No.	M.W.	Formula	Compound Name[a]	Molecular Structure	Ref.
Highly *Abundant FHT*-RNAi Metabolites					
1	326.6	$C_{22}H_{46}O$	Straight-chain primary alcohols	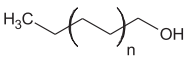	b,d,e,g
2	382.7	$C_{26}H_{54}O$			d,e, g
3	396.7	$C_{27}H_{56}O$			
4	410.7	$C_{28}H_{58}O$			b,d,e, g
5	424.8	$C_{29}H_{60}O$			b,d
6	242.4	$C_{15}H_{30}O_2$	Saturated fatty acids		c, d, g
7	340.6	$C_{22}H_{44}O_2$			c, d,e, g
8	354.6	$C_{23}H_{46}O_2$			b, d
9	368.6	$C_{24}H_{48}O_2$			c, d,e, g
10	410.7	$C_{27}H_{54}O_2$			
11	270.5	$C_{17}H_{34}O_2$	Methyl palmitate	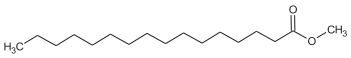	
12	294.5	$C_{19}H_{34}O_2$	Methyl linoleate	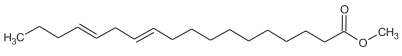	
13	180.1	$C_6H_{12}O_6$	Glucose	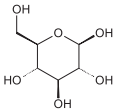	d
14	330.5	$C_{19}H_{38}O_4$	Palmitoyl glycerol (glycerol monoacyl fatty acid)	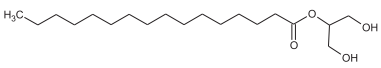	b, c, d
Highly Abundant WT Metabolites					
1	296.6	$C_{21}H_{44}$	*n*-Alkanes		c, b, d
2	324.6	$C_{23}H_{48}$			d
3	352.7	$C_{25}H_{52}$			d
4	380.7	$C_{27}H_{56}$			b, d, e
5	408.8	$C_{29}H_{60}$			d
6	438.8	$C_{30}H_{62}O$	Triacontanol (Straight-chain primary alcohol)	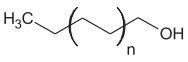	b, e
7	256.4	$C_{16}H_{32}O_2$	Saturated fatty acids		c, d, g
8	284.4	$C_{18}H_{36}O_2$			c, d, g
9	[f] 280.4	$C_{18}H_{32}O_2$	Linoleic acid (Unsaturated fatty acid)	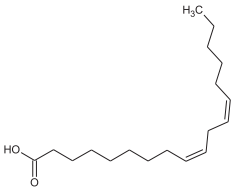	c, d
10	180.1	$C_9H_8O_4$	Caffeic acid	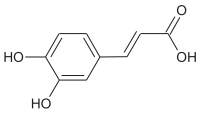	b, d, e
11	218.2	$C_{10}H_{18}O_5$	2-hydroxydecanedioic acid	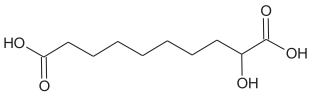	c

[a] 25 out of 31 non-polar metabolites were identified from GC-MS data using GCMSsolution software to access the NIST 2008 and Wiley 2009 mass spectral libraries.
[b] Metabolites identified by Huang et al. (2017) in non-polar extracts from native periderms of four potato cultivars (Atlantic, Chipeta, Norkotah Russet, Yukon Gold).
[c] Metabolites identified by Dastmalchi et al. (2015) in non-polar extracts from wound periderms of four cultivars (Atlantic, Chipeta, Norkotah Russet, Yukon Gold).
[d] Metabolites identified by Yang and Bernards (2007) in non-polar extracts from wound periderms (Russet Burbank).
[e] Metabolites identified by Serra et al. (2010) in wax compound from potato native periderm (Desirée).
[f] Metabolites identified by Graça and Pereira (2000) in depolymerization compounds from potato native periderm.
[g] Up-regulated metabolites identified in FHT-RNAi wound healing samples (Table 3).

caffeic acid, fatty acids (C16:0, C18:0, C18:2), 2-hydroxydecanedioic acid and triacontanol. To put these findings into context, all 76 non-polar identified metabolites are listed in Table S2.

Non-polar extracts from day-14 wound periderms were compared analogously. Unlike the polar wound extracts, the non-polar extracts showed distinct compositional features for *FHT*-RNAi and WT (Fig. 3). Differentially accumulated metabolites could be identified by the OPLS-DA method (Table 3). The up-regulated metabolites in *FHT*-RNAi 14-day wound periderm included saturated fatty acids (C8, C12, C14, C15, C17, C18, C22, C24, C26), long-chain primary alcohols (C20, C22, C24 C26, C28), alkanes (C21, C23, C25, C27, C29), glycerol monoacyl fatty acids (C18, C22) and a sterol. Only fatty acids (C16:0, C18:1, C18:2) were found as the most abundant metabolites characteristic of wound WT. All 76 non-polar

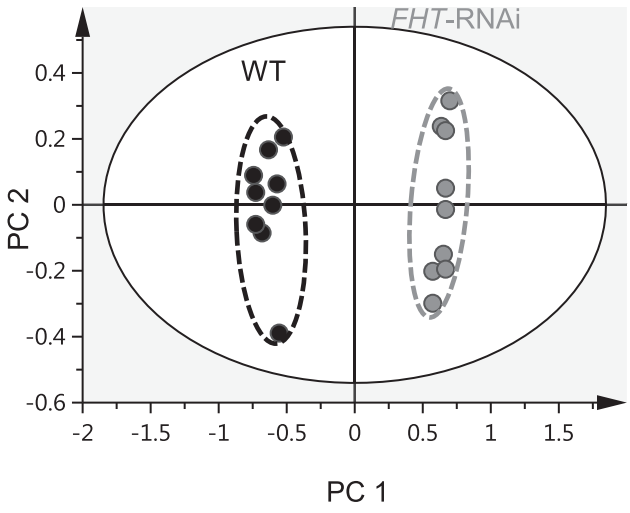

Fig. 3. PCA score plots for metabolomic analysis of non-polar extracts (GC-MS) from WT and *FHT*-RNAi wound-healing periderms, with 9 biological replicate clusters color-coded for WT (black) and *FHT*-RNAi (gray). Wound-healing samples were obtained at day 14 post wounding. The x and y axes represent the score values of principal components 1 and 2, respectively.

identified metabolites appear in Table S2. Feruloyl esters could not be identified using the GC-MS protocol, so we used higher temperatures during GC in an effort to separate and detect these compounds. They were identified by GC-MS and quantified by GC-FID using 5 WT and 3 *FHT*-RNAi replicates, respectively. As expected in light of the established FHT enzymatic function as a feruloyltransferase, the current analyses confirmed a reduction of ferulate esters in the wound periderm and an increase of primary alcohols and fatty acids when compared with WT (Fig. 4) as reported for methanolysates from native periderm (Serra et al., 2010).

2.1.3. The insoluble interfacial residue

Insoluble suspensions at the interface of the polar and non-polar extracts, obtained as described in the Materials and Methods section, were treated to remove the unsuberized tissue and the embedded waxes, and then analyzed by direct-polarization (DPMAS) ^{13}C NMR (Fig. 5). Referring to prior literature, we assigned the major structural groupings to chemical shift ranges in the spectra as follows: carboxyls or amides (COO or CONH = COX; 160–180 ppm), alkenes and arenes (92–160 ppm), partially resolved alkoxy groups (CHO, CH_2O, CH_3O; 44–92 ppm), and long-chain methylenes (-$(CH_2)_n$; 10–44 ppm) (Garbow et al., 1989; Järvinen et al., 2011; Pascoal Neto et al., 1995; Serra et al., 2014). Highly reproducible spectra, albeit with broad features attributable

Table 3
Differentially Accumulated metabolites[a] by chemical class and structure for non-polar extracts from Day-14 wound healing periderms.

No.	M.W.	Formula	Compound Name	Molecular Structure	Ref.
Highly Abundant *FHT*-RNAi Metabolites					
1	298.3	$C_{20}H_{42}O$	Straight-chain primary alcohols	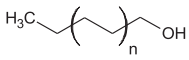	b, d
2	326.3	$C_{22}H_{46}O$			b, d, e, g
3	354.4	$C_{24}H_{50}O$			b, d, e
4	382.4	$C_{26}H_{54}O$			b, d, e, g
5	410.4	$C_{28}H_{58}O$			b, d, e, g
6	144.1	$C_8H_{16}O2$	Saturated fatty acids	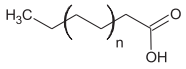	b
7	200.2	$C_{12}H_{24}O_2$			b, d
8	228.2	$C_{14}H_{28}O_2$			b, c, d
9	242.2	$C_{15}H_{30}O_2$			b, c, d, g
10	270.2	$C_{17}H_{34}O_2$			b, c, d
11	284.2	$C_{18}H_{36}O_2$			b, c, d, e
12	340.3	$C_{22}H_{44}O_2$			b, c, d, g
13	328.3	$C_{24}H_{48}O_2$			c, d, e, g
14	396.4	$C_{26}H_{52}O_2$			b, d, e
15	324.4	$C_{23}H_{48}$	n-Alkanes		b, d
16	338.4	$C_{24}H_{50}$			
17	352.4	$C_{25}H_{50}$			b, d
18	358.3	$C_{21}H_{42}O_4$	Glycerol monoacyl fatty acid	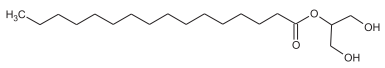	b, c, d, f
19	414.4	$C_{25}H_{50}O_4$			f
20			Sterols Beta-sitosterol Stigmasterol Cycloarlenol		a
Highly Abundant WT Metabolites					
1	256.4	$C_{16}H_{32}O_2$	Saturated fatty acids		b, d
2	280.4	$C_{18}H_{32}O_2$			b, c, d
3	282.4	$C_{18}H_{34}O_2$	Oleic acid (Unsaturated fatty acid)	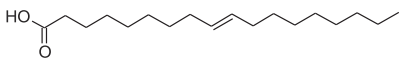	b, c, d

[a] 23 out of 30 non-polar metabolites were identified from GC-MS data using GC-MS solution software to access the NIST 2008 and Wiley 2009 mass spectral libraries.
[b] Metabolites identified by Huang et al. (2017) in non-polar extracts from native periderms of four potato cultivars (Atlantic, Chipeta, Norkotah Russet, Yukon Gold).
[c] Metabolites identified by Dastmalchi et al. (2015) in non-polar extracts from wound periderms of four cultivars (Atlantic, Chipeta, Norkotah Russet, Yukon Gold).
[d] Metabolites identified by Yang and Bernards (2007) in non-polar extracts from wound periderms (Russet Burbank).
[e] Metabolites identified by Serra et al. (2010) in wax compound from potato native periderm (Desirée).
[f] Metabolites identified by Graça and Pereira (2000) in depolymerization compound from potato native periderm.
[g] Up-regulated metabolites identified in *FHT*-RNAi native periderms (Table 2).

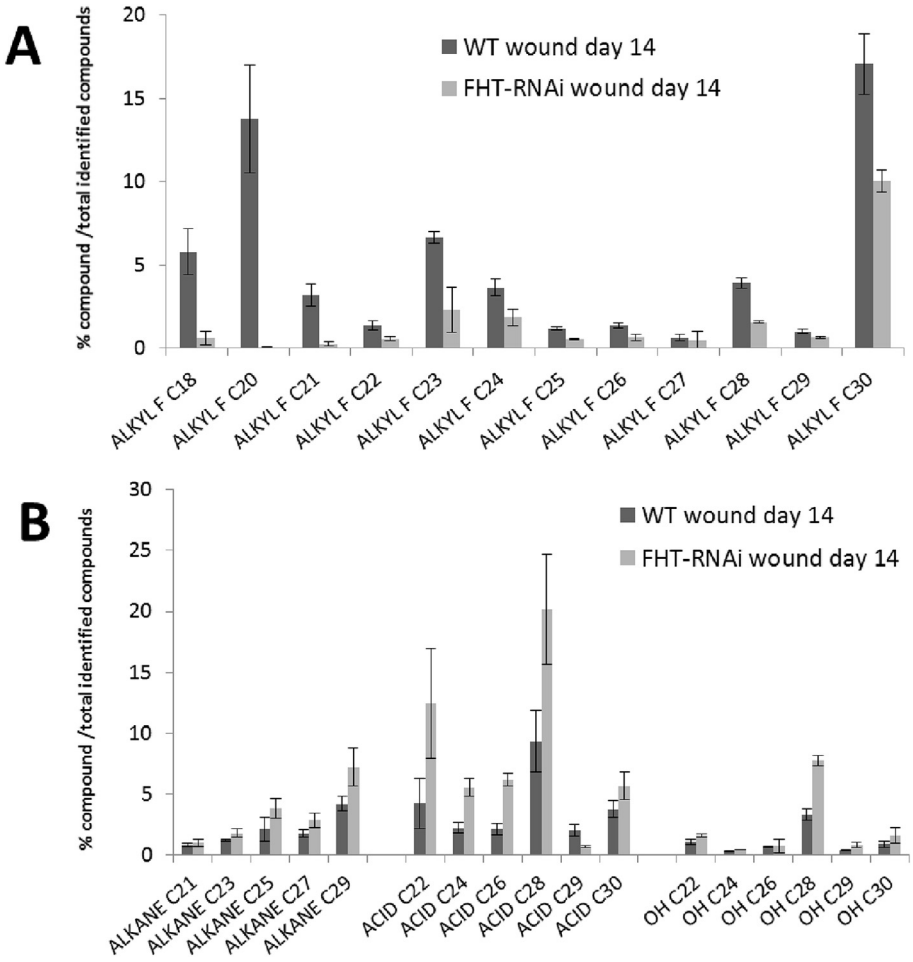

Fig. 4. Relative amounts of compounds detected by GC-FID in non-polar extracts of day-14 wound-healing periderm from *FHT*-RNAi and WT tubers. A: Alkyl ferulate esters of primary alcohols. B: Alkanes, free fatty acids and primary alcohols (OH). The carbon chain length of the fatty-acid derived compound is shown (Cpm). Each value represents the mean ± SD for *FHT*-RNAi line 37 (n = 5) and WT (n = 3).

to the chemical heterogeneity and amorphous nature of these materials, were obtained using three biological replicates each of the WT and *FHT*-RNAi periderms.

Notably different relative ^{13}C NMR signal intensities and corresponding functional group proportions were evident from these quantitatively reliable spectra. To estimate the relative numbers of each major carbon structural type, peak area ratios were compared within each DPMAS spectrum so that any unintentional variations in instrumental setup or sample mass could be avoided. The compositional trends were informative regarding the compatibilities of the suberin polymers with either the waxy overlayer or the underlying cell walls. These results are summarized in Fig. 6 (left) as ratios of carboxyls and amides (COX), alkene and arene groups, or the CH_nO alkoxy groups with respect to the long-chain aliphatic methylene groups that are expected to interact hydrophobically with waxes to confer waterproofing. Compared to WT, the *FHT*-RNAi native residue displayed an enhanced hydrophilic-to-hydrophobic balance, validated by ratios of alkene- and arene-to-$(CH_2)_n$ and alkoxy-to-$(CH_2)_n$ that were elevated by 60% and ~80%, respectively. Moreover, the degree to which polymeric suberin is deposited within the cell wall is indicated in Fig. 6 (right) by ratios with respect to the principal polysaccharide CHO groups (65–78 ppm). The residues from *FHT*-RNAi displayed significantly diminished peak area ratios for carboxyls and amides (COX), alkenes and arenes, and -$(CH_2)_n$ groups.

The distinctive *FHT*-RNAi ratios involving arenes, which were also reported for intact dewaxed suberized periderms (Serra et al., 2014), prompted us to look more closely at the aromatic suberin domain by analyzing the ether-linked breakdown products using thioacidolysis conducted after suberin depolymerization (Fig. 7, top). For both *FHT*-RNAi and WT, we detected guaiacyl (G) and syringyl (S) units but no *p*-hydroxyphenyl (H) units (Fig. 7, top), in agreement with thioacidolysis products analyzed previously by Lapierre et al. (1995) and with intact polymers examined by Yan and Stark (2000). For WT periderm, the estimated proportions of G (62%) and S units (38%) were also in rough accordance with the G (65%) and S unit (35%) content reported previously for potato native periderms using the same methodology (Lapierre et al., 1995). *FHT*-RNAi produced more abundant G units and less abundant S units than WT (Fig. 7, middle), although the differences in the S units were not statistically significant. However, the *FHT*-RNAi G/S ratio was about twofold larger than in WT (Fig. 7, bottom), suggesting a diminished cross-linking capacity of aromatic suberin polymeric structures in the FHT genetically modified tissue.

As regards the day-14 wound periderms, the interfacial dewaxed residues exhibited resonances corresponding to the same major chemical groupings as the native suberized cell walls but modestly better resolution of the ^{13}C NMR DPMAS spectra (Fig. 5, right). As in native periderms, the compositional trends in the *FHT*-RNAi wound residue displayed alkene and arene-to-$(CH_2)_n$ and

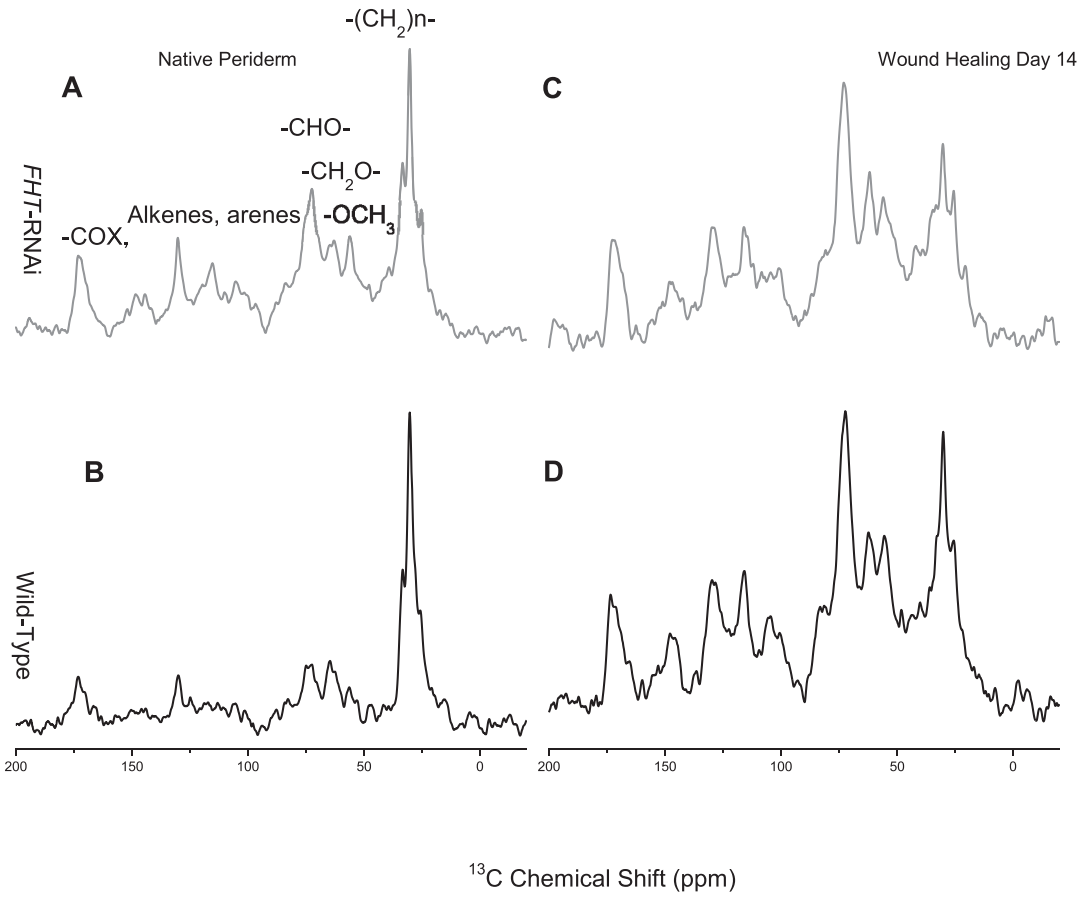

Fig. 5. 150 MHz DPMAS ^{13}C NMR spectra of suberin-enriched interfacial residues from native (A, B) and 14-day wound (C, D) periderms, color-coded for WT (black) and *FHT*-RNAi (gray) cultivars. The functional groups are assigned as carboxyl and amide groups (COO and/or CONH, 160–180 ppm); multiply bonded (alkenes and arenes, 92–160 ppm); oxygenated aliphatic carbon groups (CHO + CH_2O + CH_3O, 44–92 ppm); long-chain methylene groups (-$(CH_2)_n$-, 10–44 ppm).

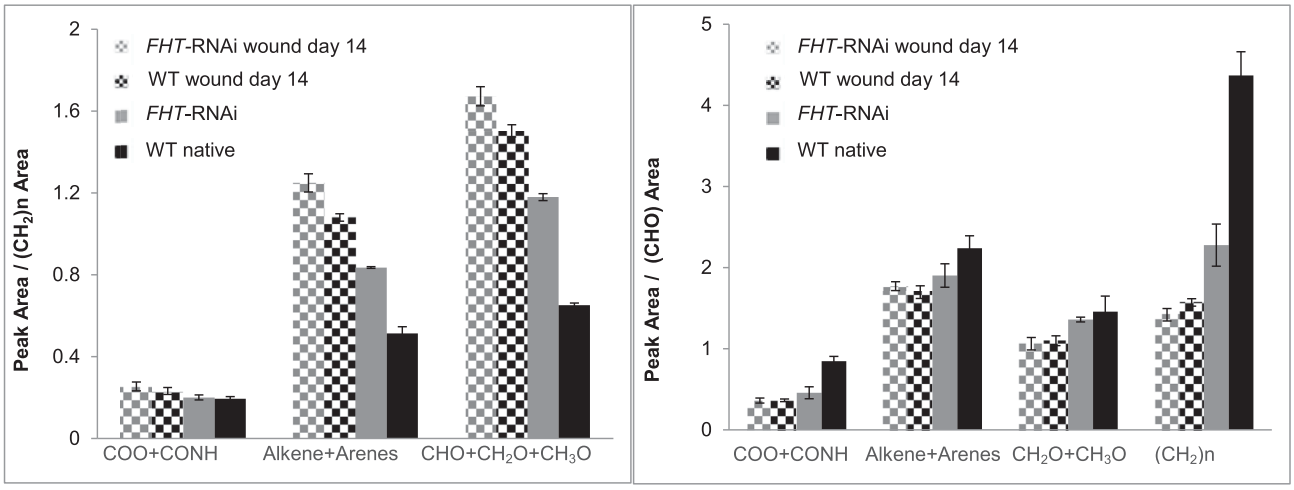

Fig. 6. Ratios of carbon-containing functional groups in the dewaxed interfacial residue of WT (black) and *FHT*-RNAi (gray) potato periderms with respect to long-chain methylene aliphatics (left) and the principal polysaccharide CHO groups (65–78 ppm) (CHO) (right), derived from 150 MHz DPMAS ^{13}C NMR spectra. Mean values and standard error bars are based on two measurements conducted on a single NMR sample.

alkoxy-to-$(CH_2)_n$ ratios that exceeded the values for WT (Fig. 6 (left)), indicating an enhanced hydrophilic-to-hydrophobic balance. However, only minor differences between WT and day-14 *FHT*-RNAi wound periderms were observed for the ratio of $(CH_2)_n$ groups to the primary polysaccharide CHO group (65–78 ppm), in contrast to the trend for native periderm (Fig. 6, right).

2.2. Native versus wound periderm

Metabolites present in extracts from freshly harvested (immature) native and 14-day post-wounding disks were compared in each of the WT and *FHT*-RNAi varieties. With respect to the polar metabolites, a PCA-based comparison between native and wound

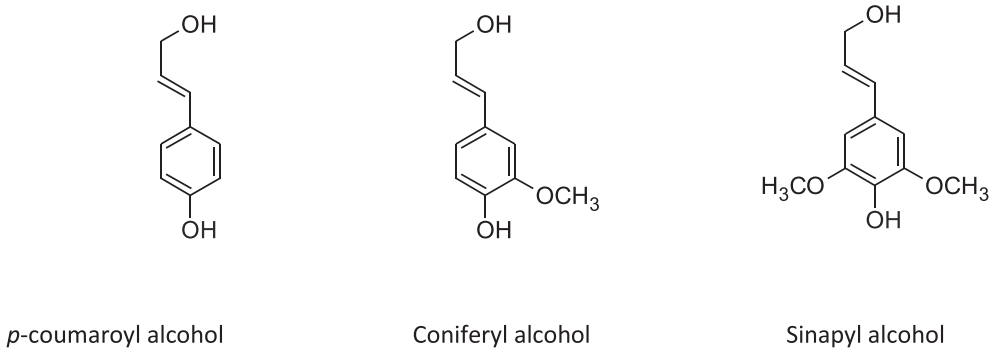

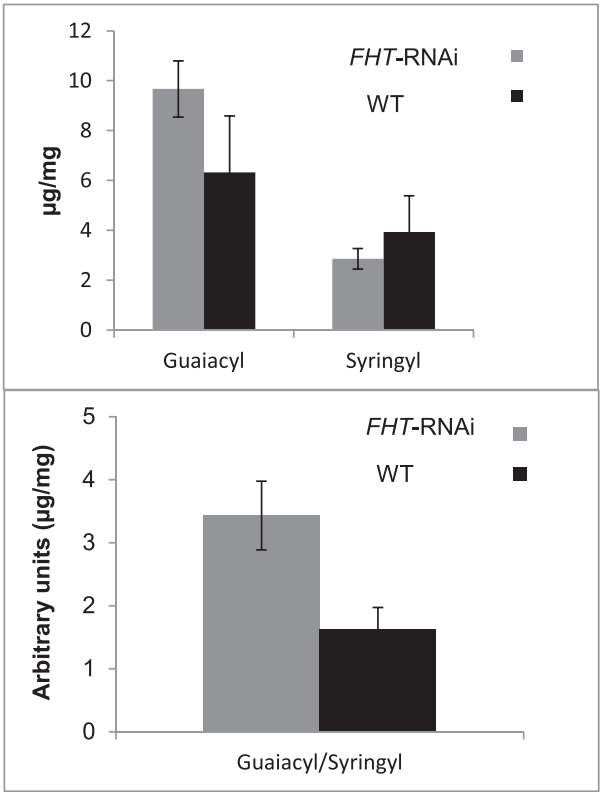

Fig. 7. Amounts and proportions of phenylpropanoid building blocks in native potato periderms from WT and *FHT*-RNAi tubers. Mean values and standard deviation error bars are based on the peak areas of the identified guaiacyl and syringyl units in GC-MS. Top: chemical structures of major aromatic groups released by thioacidolysis; Middle: amounts of guaiacyl and syringyl units per mg of dry periderm tissue; Bottom: ratio of guaiacyl to syringyl units in periderms.

periderms was precluded by the higher overall concentration and much larger number of detectable metabolites in the native extracts. However, direct comparison of the LC traces revealed distinctive features of wound periderm in terms of the major chemical classes represented among the metabolites (Fig. 8 and Table S1). Five metabolites predominate in both WT and *FHT*-RNAi wound polar extracts: caffeoylputrescine (retention time (RT) 11.8 min), feruloylputrescine (RT 14.8 min), α-chaconine (RT 28.5 min), α-solanine (RT 29.0 min), and a feruloyloctopamine-feruloyloctopamine (FO-FO) dimer (RT 31.7 min). Peaks with retention times of 21.3–25.5 min were significantly diminished in both varieties of wound periderms, corresponding to a paucity of flavonoid glycosides (aglycones of tetrahydroxyflavonoids at *m/z* 903 and 933 with fragments 449, 287, and 269; luteolin-7-O-rutinoside at *m/z* 593) and phenolic polyamines containing more than two cinnamic acid derivatives (dihydrocaffeoyl spermines at *m/z* 721 and 723 with fragments 529, 407, and 191). For the non-polar metabolites, PCA-based comparisons of native and wound extracts were again precluded by disparities in overall concentration and number of detectable metabolites. However, it was possible to compare the respective potential biomarkers that discriminate between WT and *FHT*-RNAi in native (Table 2) and wound (Table 3) periderms. With respect to the corresponding WT periderms, both *FHT*-RNAi native and wound periderms had the same families of up-regulated metabolites. However, whereas alkanes were up-regulated in WT native periderms, those metabolites were up-regulated in *FHT*-RNAi wound. Moreover, abundant sterol biomarkers were observed uniquely in the *FHT*-RNAi wound periderm (Table 3).

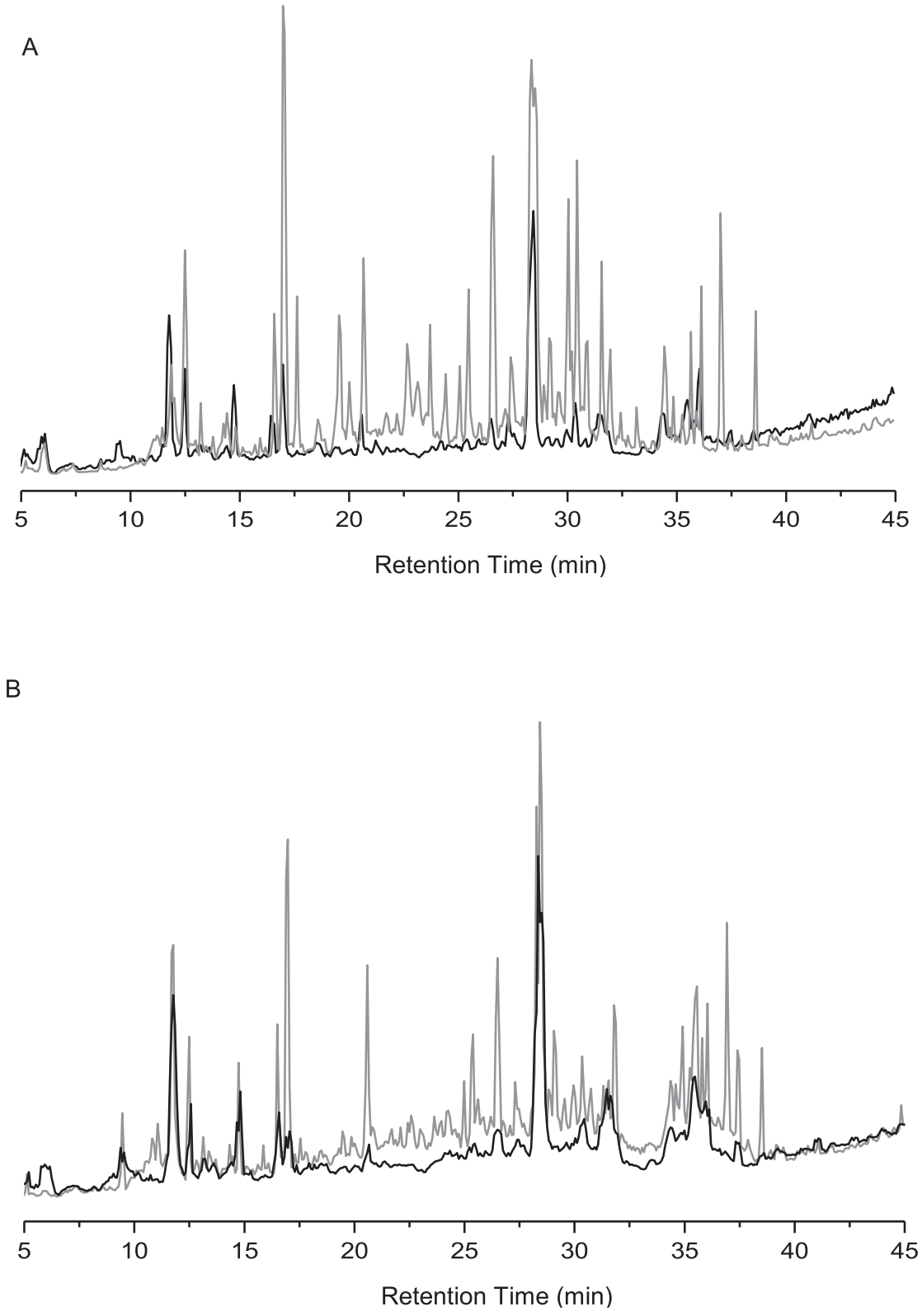

Fig. 8. Overlay of typical LC-MS traces for native (gray) and day-14 wound (black) polar potato periderm polar extracts. A: WT native vs. WT day-14 wound; B: *FHT*-RNAi native vs. *FHT*-RNAi day-14 wound.

2.3. Wound healing time course in FHT-RNAi and WT potato discs

As noted in the Introduction, wound healing to restore the chemical and physical barriers in fruits and tubers is a complex process that proceeds in distinct steps. To compare the wound healing time course in WT and *FHT*-silenced tubers, we undertook parallel studies of polar and non-polar soluble metabolites along with polymeric solid composites at four key time points: immediately after wounding (day 0), when a closing layer has formed (day 3), when a new wound periderm is nascent (day 7), and when the new periderm has developed but is still immature (day 14) (Lulai et al., 2016).

For polar soluble metabolites, Fig. 9 shows a score plot from LC-MS-based multivariate analysis. Clustering indicates good consistency of the compositional data from each set of biological replicates. The largest variations with time occurred for principal component 1 (PC1) from day 0 to day 3; smaller changes, primarily in PC2, were observed from day 3 to days 7 and 14. The *FHT*-RNAi and WT polar extracts exhibited distinct profiles at day 0 with respect to other time points, and each variety of exposed wound tissue exhibited a similar compositional progression during the healing process. OPLS-DA pairwise analysis during the course of healing (comparing each pair of time points) revealed no significant compositional differences between days 7 and 14 for either WT or *FHT*-RNAi. In contrast, when comparing day 3 and day 7, we found that both WT and *FHT*-RNAi day-7 extracts were richer in α-chaconine and α-solanine glycoalkaloids, whereas only day-3 WT extracts were richer in feruloyloctopamine.

To evaluate the impact of FHT silencing on the wound-healing process, pairwise comparisons of WT vs. *FHT*-RNAi were made for polar extracts at each of days 0, 3, 7 and 14 by PCA and OPLS-DA methods. No statistically significant differences in the overall metabolite profiles could be verified despite the appearance of day-0 variations in PC2 (Fig. 9): a negative value of Q^2 in the PCA modeling showed that the variation among biological replicates was comparable to differences between the two types of wound-healing periderm. Neither were there compositional differences between any of the non-polar extracts, with the exception of day 14, for either WT or for *FHT*-RNAi tissues (data not shown).

The DPMAS ^{13}C NMR spectra of the interfacial residues isolated at days 0–14 are shown in Fig. S5. At day 0, residues are essentially comprised of polysaccharides since the region between 45 and 108 ppm is contributed primarily by cell walls. At days 3, 7, and 14, key resonances attributable to the suberin aliphatic polyester appear with increasing prominence as reported previously (Stark et al., 1994): chain methylene groups, carbonyl groups, alkenes, and arenes. A quantitative analysis of the corresponding DPMAS spectra yields ratios for day-3, day-7 and day-14 residues, each measured with respect to the major polysaccharide peak of the cell-wall CHO region (Fig. S6). At day 3, the spectral regions attributable to the suberin (10–44, 108–160, 160–180 ppm) exhibit larger relative contributions in *FHT*-RNAi. At day 7, the difference between *FHT*-RNAi and WT in the corresponding ratios diminishes, and at day 14 WT shows nearly the same ratios as *FHT*-RNAi (Fig. S6, Fig. 6 (right)).

3. Discussion

3.1. FHT deficiency in native vs wound periderms

By conducting the analysis of extracted metabolites and the solid interface holistically, the current work also complements prior studies of FHT deficiency in native periderms that were made by examination of soluble waxes, soluble monomeric suberin breakdown products, and polymeric solids (Graça, 2015; Serra et al., 2014; Serra et al., 2010). As expected from its demonstrated role as a feruloyl transferase in native periderm, *FHT* down-regulation in wound periderm leads to diminished amounts of non-polar alkyl ferulates (reaction products) and augmented amounts of primary alcohols (reaction substrates) (Fig. 3B; Tables 2 and 3), thus

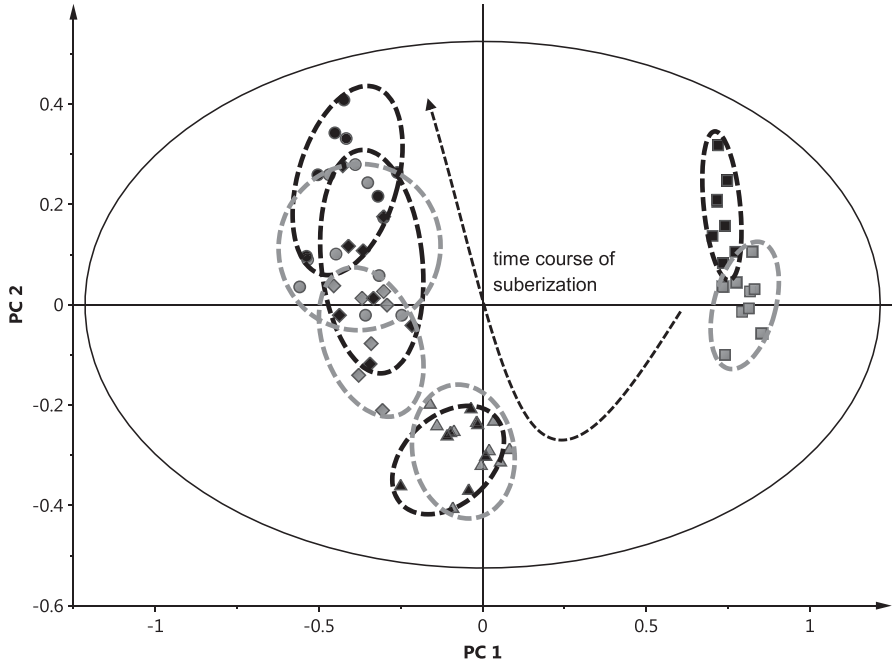

Fig. 9. PCA score plot of negative-mode LC-MS data used in metabolomic analysis of polar extracts from wound-healing potato parenchyma (day 0) and wound-healing tissues (days 3–14), showing 9 biological replicates color-coded for WT (black) and *FHT*-RNAi (gray) tubers. The numbers of days after wounding are denoted by squares (0), triangles (3), diamonds (7), and circles (14), respectively. Differences between the WT and *FHT*-RNAi day-0 extracts are not statistically significant (see text).

extending the role for this enzyme to the wound-healing process. However, the impact of *FHT* silencing on the wound-healing response does not invariably conform to the findings for native periderm. Thus for the polar metabolites, higher levels of phenolic polyamines are observed preferentially only for the *FHT*-RNAi native periderm (Table 1). As regards the non-polar metabolites, in FHT-deficient tubers the saturated fatty acids and glycerol monoacyl fatty acids increase in both native (Table 2) and wound periderms (Table 3), although the wound periderm shows a broader distribution of fatty acid chain lengths. Conversely, alkanes are abundant in *FHT*-RNAi wound but diminished in the corresponding native periderm (Fig. 4, Tables 2 and 3) (Serra et al., 2010), whereas sterols are more abundant only in FHT-deficient wound periderm (Table 3).

For the interfacial polymeric solids, both the native and day-14 wound FHT-deficient periderms have larger alkene/arene and alkoxy proportions with respect to long-chain methylene groups. The latter ratio (alkoxy/long-chain methylene groups) and diminished contributions from $(CH_2)_n$ moieties demonstrates an augmented hydrophilic-hydrophobic balance (Fig. 6, left) and provides a rationale for the enhanced permeability of the *FHT*-RNAi native periderm (Serra et al., 2010). On the other hand, in the native periderms a diminished propensity for suberin deposition within the cell wall of FHT-deficient periderms is inferred from the proportions of $(CH_2)_n$ moieties with respect to CHO groups, confirming prior observations for unextracted samples (Fig. 6, right; (Serra et al., 2014). The alkene- and arene-to-CHO ratio is also diminished in the native periderm solids, though the aromatic functional groups are retained strikingly in the recalcitrant residue remaining after suberin depolymerization (Serra et al., 2014).

This last compositional trend is extended by the finding of relatively greater G-unit content for groups linked through β-O-4 (labile alkyl-aryl ether) bonds in native *FHT*-RNAi (Fig. 7), supporting facilitated linkage by oxidative coupling of ferulic-type units in the lignin-like polymeric structures and/or architectural alterations that promote the release of these G units upon thioacidolysis. Recent FT-IR analyses of wax-free periderms (Graça, 2015) have also shown enhanced G content in *FHT*-RNAi compared with WT. The greater proportion of labile β-O-4 linked G units in the *FHT*-RNAi polymer correlates additionally with the finding of larger amounts of feruloyl polyamines in the polar extracts. When incorporated within the cell wall, such structures result in reinforcement and stiffening (Bassard et al., 2010), in agreement with the greater stiffness and the compromised mechanical strength of the *FHT*-RNAi periderm reported previously (Serra et al., 2014). However, our analysis does not probe the enrichment in terminal or internal G-units or the presence of other thioacidolysis-resistant types of inter-unit bonds (β-1, β-β, β-5, 4-0-5 and 5-5 linkages) (Lapierre et al., 1996; Négrel et al., 1996), which could also affect the cross-linking capacity and associated mechanical properties of the *FHT*-RNAi periderm. Taken together, the changes induced by FHT down-regulation in native and wound periderms nonetheless demonstrate many common features of their biosynthetic pathways.

The current analyses, together with related prior work on aliphatic suberin breakdown products, allow us to infer both direct consequences of alkyl ferulate blockage and indirect effects of dehydration stress as depicted in Fig. 10 (Bernard et al., 2012; Bernards, 2002; Fraser and Chapple, 2011; Matsuda et al., 2005; Serra et al., 2010; Yang et al., 2010; Yang and Bernards, 2006). Since *FHT* silencing blocks the esterification of ferulic acid to ω-hydroxyfatty acids or alcohols, elevated levels of primary long-chain alcohols in the non-polar extracts and up-regulation of suberin-associated waxes in *FHT*-RNAi native periderm (Serra et al., 2010) are expected. However, the ω-hydroxyfatty acid substrates are not found abundantly. Thus, these latter substrates could react to form α,ω-diacids and then be converted efficiently to glycerol esters via the catalytic action of CYP86 family members, GPAT5, and GPAT7 enzymes, a hypothesis supported by our finding of a highly abundant glycerol monoacyl fatty acid in FHT-RNAi periderms (Tables 2 and 3). These intermediates can ultimately be incorporated into suberin, but their elevated levels can also have a negative feedback effect that decreases the level of ω-hydyroxyacids among the aliphatic suberin breakdown products (Serra et al., 2010) and accounts for the abundant LC and VLC fatty acids in extracts from the *FHT*-RNAi periderms. It is also noteworthy that accumulation of alkanes is favored in *FHT*-RNAi wound periderm but diminished in *FHT*-RNAi native periderm, compared with the respective wild types.

Turning to the feruloyl-CoA precursor that is blocked from esterification in *FHT*-RNAi periderms, the changes observed for metabolites in both soluble polar extracts and insoluble cell-wall polymers exemplify the possibility of ferulic acid uptake via multiple biochemical processes and support the cross-talk proposed for pathways involving alkyl ferulates, cell-wall monolignols and hydroxycinnamates, and hydroxycinnamic acid amines in potato periderms (Bernards, 2002; Graça and Santos, 2007; Matsuda et al., 2005). In addition to the rerouting of feruloyl-CoA to feruloylputrescine and related amides, it is interesting to highlight the concurrent channeling of caffeoyl-CoA to caffeoylputrescine. Both reactions are catalyzed by the same putrescine hydroxycinnamoyltransferase enzyme (PHT) (Matsuda et al., 2005), suggesting that the presence of feruloyl-CoA and/or the dehydration-induced stress can act as positive regulators of PHT in native periderms. The latter rationale also dovetails with our recent finding of elevated caffeoylputrescine accumulation in highly permeable native Norkotah Russet potato periderms, as compared with smooth Yukon Gold cultivars (Huang et al., 2017).

3.2. Phenolic polyamines and russeted potato skins

The role of polyamines in wound periderm has been a matter of longstanding discussion. Phenolic amines can combine the growth and development regulatory functions of polyamines (Martin-Tanguy, 1985) with the toxic free radical scavenging, antioxidative, and wall-strengthening properties conferred by hydroxycinnamic acids (Volpert et al., 1995; among others). It was suggested by (Heng et al., 2016) that the H_2O_2 generated during polyamine metabolism might contribute to russet formation on the exocarp of pear fruits. A role as cross-linked intermediates putatively involved in the suberization process was suggested by King and Calhoun (King and Calhoun, 2005, 2010) for feruloyl amides and cross-linked dimers in potato scab lesions.

FHT deficient tubers (cv. Desirée) show a distinctive russeted skin that is more rigid, fragile, and prone to microfissure and has increased water permeability in contrast with the smooth WT tubers (Serra et al., 2010). Moreover, the native FHT-deficient periderm accumulates phenolic amines such as caffeoylputrescine, feruloylputrescine and feruloyloctopamine compared with WT (Table 1). Notably, potatoes with russeted skin display increased water permeability (Ginzberg et al., 2012; Lulai and Orr, 1994) and phenolic polyamines are notably abundant in native and wound periderms from russeted Norkotah and Atlantic potato cultivars (Dastmalchi et al., 2014; Huang et al., 2017). In this regard (Landgraf et al., 2014), have made an interesting observation: in tubers (cv. Desirée) silenced for an ABC transporter (StABCG1), a decrease in suberin amount and an increase in water permeance are associated with abundant levels of phenolic amines and russeted skin appearance. Taken together, the above considerations suggest that a certain degree of water loss inherent in the *FHT*-RNAi

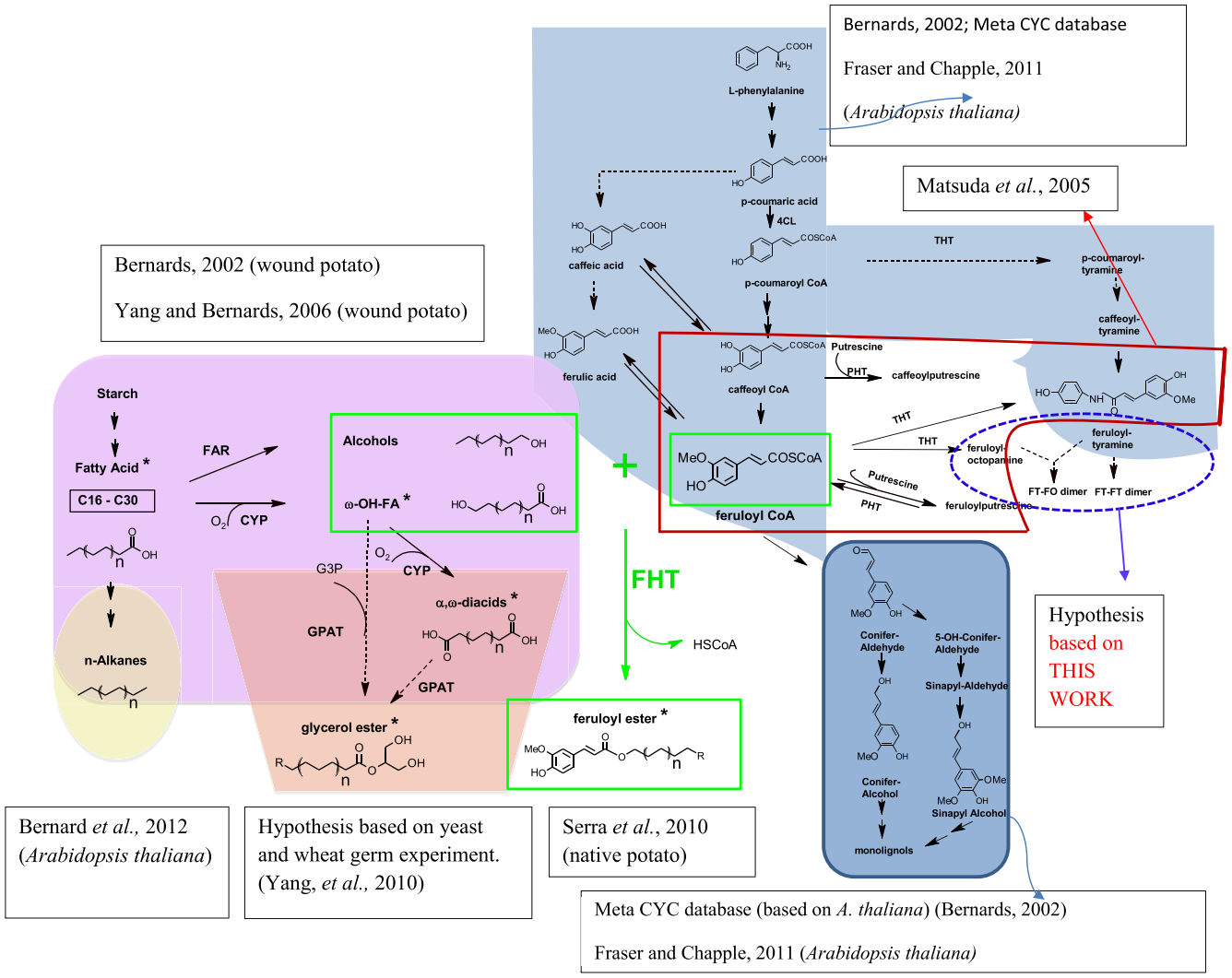

Fig. 10. Proposed biosynthetic pathways for suberized potato periderms. (Bernards, 2002; Matsuda et al., 2005; Yang and Bernards, 2006; Serra et al., 2010; Yang et al., 2010; Bernard et al., 2012; Graça, 2015). Reactions denoted by solid lines have been derived from the indicated references, while those denoted by broken lines are hypothetical or assumed.

tuber skin may induce higher levels of phenolic polyamines and a russeted periderm appearance.

3.3. *FHT* deficiency affects soluble metabolites and polymeric solids formed during wound healing

One perspective on healing differences in FHT deficient and WT tubers comes from disparities in the progress of suberin deposition, reported by ratios of particular functional groups measured in solid-state DPMAS ^{13}C NMR spectra of the solid interfacial layer. As shown in Fig. S6 with respect to the polysaccharide cell-wall CHO resonances, all structural moieties present in the interfacial solid accumulate more rapidly during the first 3 days in *FHT*-RNAi wound periderms. During the following days, suberin deposition occurs more vigorously for the WT until it "catches up" or surpasses the *FHT*-RNAi at day 14. Considering that *FHT*-RNAi wound periderm has knocked down transferase enzymatic activity for the aliphatic constituents, a diminished rate of development for both arene and aliphatic constituents of the suberin biopolymer should be expected. Nonetheless, the early deposition of suberin in the *FHT*-deficient wound periderm could be explained by a baseline condition of water stress in the tuber parenchyma prior to wounding, associated in turn with the greater rate of water loss of the *FHT*-RNAi periderm (Serra et al., 2014). This state of hydric stress could induce a protective response that overlaps with the wound response. However other alternative explanations, such as the formation by day 3 of different polymeric structures in *FHT*-RNAi compared with WT, cannot be ruled out.

A contrasting perspective emerges from consideration of the pools of soluble metabolites in wound-healing tissues. Differences between the non-polar extracts are found only in the day-14 wound periderm, where the knocked down feruloyl transferase activity is evident in the abundant long-chain fatty acids and fatty alcohols (reactants) and the diminished ferulate esters (products). For the polar extracts, some differences between *FHT*-RNAi and WT are evident immediately after wounding (day 0) but subsequently, both wound periderms experience an overall compositional convergence (from day 3 onwards, Fig. 7). Surprisingly, at day 0 there is a greater accumulation of caffeoylputrescine in *FHT*-RNAi compared with WT. Given that the FHT protein does not accumulate and that the gene promoter is not expressed in the tuber parenchyma (Boher et al., 2013), the abundance of phenolic polyamines in the newly exposed wound tissue (day 0) of the *FHT*-RNAi tubers should be unrelated to blockage of FHT but rather viewed as

a constitutive feature of the *FHT*-RNAi tubers. Plausibly, the hydric stress produced by the 14-fold greater water loss in periderms of *FHT*-RNAi tubers (Serra et al., 2010) causes a permanent stress within the inner fleshy tissues, which in turn could induce the synthesis of radical scavenging phenolic polyamines as a defense mechanism (Bassard et al., 2010).

4. Conclusions

These 'holistic' analyses encompass soluble metabolites, solid polymer composites, and breakdown products from diverse chemical treatments of *FHT*-deficient immature native and wound periderms compared with WT. Both *FHT*-RNAi periderms show an augmented hydrophilic-hydrophobic balance. A metabolic rerouting to enhance the relative amounts of phenolic polyamine structures occurs upon *FHT*-RNAi silencing only in native periderms, providing a rationale for their enhanced permeability (Serra et al., 2010) but leaving the analogous permeability trend in wound periderms unexplained. Each of these observations is also shared to different degrees by the immature native periderm of russeted potato cultivars (Huang et al., 2017) and by *ABCG1*-RNAi tubers (Landgraf et al., 2014), as well as by the scabby lesions produced by *Streptomyces scabies* (King and Calhoun, 2005, 2010). With this comprehensive molecular-level information in hand, we are now better able to understand the impact of this key biosynthetic step on the protection against crop infection and dehydration that is provided by the periderm layer.

5. Experimental procedures

5.1. Plant materials

FHT-RNAi-silenced potato plants (line 37) (*Solanum tuberosum* cv. Desirée) were obtained as described by Serra et al. (2010). *FHT*-RNAi silenced plants and the corresponding wild-type (WT) cultivar were first propagated *in vitro*: stem cuttings were cultured in Murashige and Skoog media supplemented by 2% (w/v) sucrose and placed in growth cabinets at 22 °C with a light/dark photoperiod cycle of 16/8 h for 21 days. After transfer to soil, the plants were grown in a greenhouse to form tubers that were harvested from 9-week-old plants. Harvested tubers were rinsed with tap water to remove soil particles and the tuber skin was collected using a flat spatula, taking advantage of easy peeling at this immature developmental stage and avoiding the underlying parenchymatic flesh tissue to the extent possible. The samples were frozen in liquid nitrogen, ground using a mortar and pestle, lyophilized until dry, and stored in a vacuum-sealed bag at −80 °C. Although the collected tuber skin corresponded strictly speaking to the phellem tissue, we designate the samples as native periderms (containing suberized phellem, phellogen, and phelloderm tissues) in conformance with previous reports (Franke et al., 2005; Hammes et al., 2006; Serra et al., 2014; Stark et al., 1994).

To prepare wound-healing samples from freshly harvested potato tubers (Dastmalchi et al., 2014; Pacchiano et al., 1993; Yang and Bernards, 2006), internal flesh tissues about 5 mm thick were sliced longitudinally to obtain disks and placed on wet cellulose filter paper. The healing process was accomplished inside closed humidified plastic boxes equipped with wire netting supports at 25 °C in the dark. The new brown surface layer of wound-healing tissue was excoriated and collected with a spatula at 0, 3, 7 and 14 days after wounding, corresponding to each stage of suberization: fresh cut samples, early healing in which the suberized closing layer has formed, the developing wound periderm, and well-formed wound periderm. The 3-, 7- and 14-day old wound periderms, as well as the freshly harvested native periderm used in our analyses, were susceptible to skinning. Therefore, both periderms were compared before the skin-set process that marks the transition from immature to mature periderm has taken place. In wound periderm, this phenomenon occurs about 3 weeks post-wounding (Sabba and Lulai, 2002). Upon harvest of the wound-healing materials, samples were collected by the same process as described for the native periderms and stored as dry powders. Both WT and *FHT*-RNAi samples at the day-0, day-3, day-7, and day-14 time points were collected.

5.2. Chemicals

Solvents for soluble metabolite analysis were purchased as follows: analytical grade chloroform and HPLC grade methanol from Fisher Scientific (Pittsburgh, PA); LC-MS grade water and acetonitrile from J. T. Baker (Center Valley, PA); analytical grade hexane and anhydrous pyridine from EMD Chemicals (Gibbstown, NJ). Additional reagents used in these analyses included analytical grade formic acid from Sigma-Aldrich (St. Louis, MO) used in LC-MS experiments, N-Methyl-N-(trimethylsilyl)trifluoroacetamide (MSTFA) + 1% trimethylchlorosilane (TMCS) from Thermo Scientific (Bellefonte, PA) used in GC-MS, and a C7−C40 Saturated Alkanes Retention Index Standard from Supelco (Bellefonte, PA). For removal of cell-wall materials from the solid interfacial suspension between polar and non-polar extracts, cellulase (EC 3.2.1.4; CAS No. 9012-54-8) and pectinase (EC 3.2.1.15; CAS No. 9032-75-1) were purchased from Sigma-Aldrich.

5.3. Sample preparation

Dried native periderm (~10 mg) and wound-healing tissues (~20 mg) were weighed and transferred into 4 mL glass vials. Nine replicate extracts were prepared for each WT and *FHT*-RNAi native potato periderm and each wound-healing time point. Extraction followed a published protocol (Choi et al., 2004; Kim et al., 2010; Wolfram, 2006). Briefly, 1.54 mL methanol and 0.33 mL water were added to each dried sample together with 5 small zirconia oxide beads, and the mixture was vortexed for 60 s. After addition of 0.77 mL chloroform and an additional 60 s of vortexing, the samples were shaken in an incubator for 15 min at room temperature. After addition of another 1.54 mL portion of chloroform-water (1:1 v/v), the samples were sonicated for 15 min and shaken in an incubator for another 15 min. The extraction mixtures were centrifuged at 3000 rpm for 15 min at 4 °C; a lower non-polar soluble layer, an upper polar soluble layer, and a solid interfacial suspended residue were collected separately with glass Pasteur pipettes. The non-polar portion (~1.5 mL) was divided between two 2-mL brown vials and dried in a hood at room temperature. The polar portion (~2.0 mL) was also divided between two portions, one of which was dried under nitrogen and the other kept as a liquid without further processing. All samples were stored at −20 °C for subsequent analysis by GC-MS, LC-MS, solution-state NMR, and/or solid-state NMR.

Derivatization for GC-MS analysis was conducted by dissolving the dried non-polar extract in 50 μL of dry pyridine with 80 μL of MSTFA and 1% TMCS (Yang and Bernards, 2007), then shaking in an incubator at 50 °C for 1 h and equilibrating at room temperature.

The solid interfacial residues were washed twice with distilled water and dried overnight at 50 °C, then treated with hydrolytic enzymes to remove unsuberized cellulose and pectin associated with the cell wall. The following procedures, which have been developed for 'whole' periderm tissues that were not subjected to extraction (Pacchiano et al., 1993; Serra et al., 2014), were used to produce suberin-enriched periderm residues. *Aspergillus niger* cellulase (0.1% w/v) and pectinase (0.4% v/v) were dissolved in

100 mM acetate buffers at pH 5.0 and pH 4.0, respectively. A 4-mL portion of cellulase buffer was added to each of the samples, which were shaken at 150 rpm and 37 °C for 48 h and then at 44 °C for 48 h. The completeness of cell-wall cellulose digestion using this two-step protocol was validated in two ways: by comparison of our yields (Dastmalchi et al., 2015) with the >80% losses in mass reported after 5 cellulase treatments of wound potato parenchyma plus periderm (Pacchiano et al., 1993); and by observing that no further decreases in mass of peeled potato periderms occurred upon retreatment (B. Yu, unpublished results). After rinsing twice with distilled water to remove the cellulase, 4 mL of pectinase buffer was added to each of the samples, which were shaken at 28 °C and then 31 °C for 24 h each. After rinsing three times with distilled water, the residues were dried in an oven at 50 °C overnight. Next, 24-h Soxhlet solvent extraction treatments were used to remove soluble waxes and fatty acids using refluxing methanol, chloroform, and hexane successively. Finally, the samples were dried in an oven at 50 °C for 10 h.

5.4. Solution-state NMR analysis

The polar extracts were reconstituted using a 100 mM pH 7.4 phosphate buffer in D_2O containing 0.01 mg/mL of the internal standard 4,4-dimethyl-4-silapentane-1-sulfonic acid (DSS). NMR spectra were obtained using a Bruker AVANCE PLUS spectrometer (Bruker Biospin, Karlsruhe, Germany) operating at an 800 MHz ^{1}H frequency and fitted with a cryomicroprobe for 1.7 mm o.d. sample tubes (Norell, Landisville, NJ) and an automated NMR SAMPLEJET accessory. ^{1}H NMR data were acquired at 25 °C using TOPSPIN version 3.1 software and presaturation of the residual water signal set to 4.695 ppm, a constant receiver gain, 512 scans, and a 1.0-s recycle delay between transients. The spectrum after Fourier transformation and signal conditioning had a spectral window of 14 ppm defined by 32 K data points.

5.5. Gas chromatography-mass spectrometry (GC-MS) analysis

The derivatized non-polar samples were analyzed using a Shimadzu QP2010 plus instrument (Canby, OR) equipped with an AOC-5000 automatic injection system, a RESTEK (Bellefonte, PA) Rtx®-5MS low-bleed column (fused silica, 30 m × 0.25 μm i.d.), and GCMSsolution software version 2.53. The injection temperature was set to 250 °C. A 1 μL sample was injected in splitless mode with high purity helium as carrier gas at a constant flow rate of 1 mL min^{-1} and a pressure of 61.5 kPa. The temperature program was set as follows (Yang and Bernards, 2007): after a 5 min delay at 70 °C to allow the solvent to purge the system, the oven temperature was increased to 310 °C at 5 °C/min, then held for 11 min at that temperature. The total GC run time was 64 min. Mass spectra were recorded in Electron Ionization (EI) mode from 8 to 64 min to avoid the peaks from solvent, pyridine and derivatization reagent. The scan time was 0.5 s and the scan range was *m/z* 45–600. Instrumental parameters included the ionization voltage (70 eV), ion source temperature (200 °C), and interface temperature (280 °C). The mass spectrometer was tuned with perfluorotributylamine (PFTBA) for mass calibration, performance optimization, and consistency. Three blank samples were run at the beginning, middle, and end of the experimental sequence to record the baseline, check the instrumental performance, and detect possible contamination, respectively.

5.6. Liquid chromatography-mass spectrometry (LC-MS) analysis

LC-MS of the polar extracts, for both native periderm and wound-healing samples, was carried out using an Applied Biosystems Sciex4000 QTRAP mass spectrometer (Foster City, CA) equipped with a Shimadzu UFLC system (Canby, OR) and including two LC-20 AD pumps, an SIL-20 A C automatic injector, a CBM-20 A communication bus module and a CTO-20 A C column oven. A 150 × 4.6 mm i.d. 3.0-μm reverse phase AscentisR™ C18 column (Supelco Corp., Bellefonte, PA) was used with the column oven set to 30 °C and injection volumes of 10 μL and 20 μL for native and wound periderm samples, respectively. The mobile phase consisted of (A) water containing 0.1% formic acid (v/v) and (B) acetonitrile containing 0.1% formic acid (v/v). The flow rate was 0.5 mL min^{-1} with gradient elution conducted as follows: 0–1 min: 2% B; 1–30 min: 2%–35% B; 30–45 min: 35%–98% B; 45–51 min: 98% B; 51–52 min: 98%–2% B. Electrospray ionization (ESI) mass spectra were acquired in both negative and positive ion modes for the range *m/z* 100–1300. Pressures of high-purity nitrogen gas (99.995%) were set at 50 psi for the nebulizing gas and 40 psi for the heating gas, respectively. The source temperature was 300 °C. The optimized values of spray voltage, declustering potential, and entrance potential in negative mode were −4500 V, −140 V, and −10 V, while the values in positive mode were 5500 V, 80 V, and 10 V, respectively. Analyst 1.4.2 software was used for data processing. Tandem mass spectrometric analyses (LC-ESI-MS^2 and MS^3) were conducted at four different collision energy levels for both negative mode (−35, −50, −65, and −80 eV) and positive mode (35, 50, 65 and 85 eV). Chlorogenic acid and rutin, compounds reported previously in potatoes, were used as reference standards. Blank samples were run as described for the GC-MS experiments (Dastmalchi et al., 2014; Neubauer et al., 2012).

5.7. Time-of-flight mass spectrometry (TOF-MS)

To obtain highly accurate masses of metabolites present in the potato skin, the polar extracts of potato native periderm were fractionated 4 times under the same chromatographic conditions used in the LC-MS experiments using an Agilent 1200 series HPLC system (Santa Clara, CA) equipped with a quaternary pump, helium degasser, column heater, diode array detector and analytical fraction collector. Fractions were collected from 6 to 45 min with 1 min intervals for a total time of 40 min. A Waters LCT Premier XE time-of-flight mass spectrometer (Milford, MA) was used to obtain high-resolution molecular masses, with 400 pg/L leucine enkephalin (Sigma-Aldrich, *m/z* 556.2771) as a standard. The flow rate of the reference solution was 100 μL/min. Mass spectra were acquired over the range *m/z* 100–1300 in both positive and negative modes. The desolvation gas flow was set to 800 L/h at a temperature of 350 °C, and the cone gas flow was 10 L/h. The cone and aperture voltages were set to 10 V and 25 V for negative mode, 25 V and 10 V for positive mode, respectively. The data acquisition rate was 0.15 s/scan, with a 0.01 s interscan delay using dynamic range enhancement (DRE) lock mass. Datasets were collected for 1 min each. The possible elemental compositions for each accurate mass were calculated with Masslynx 4.1 software using a monoisotopic mass type.

5.8. Processing of mass spectral data

The software package MZmine 2.4 (VTT Technical Research Center, Helsinki, Finland and Turku Center for Biotechnology, Turku, Finland; http://mzmine.sourceforge.net/) was utilized for processing of GC-MS and LC-MS chromatograms (Katajamaa et al., 2006; Pluskal et al., 2010) after conversion of the raw data into metabolomics data matrices suitable for multivariate analysis (Want and Masson, 2011). The raw GC-MS data files (.qgd) were converted into NetCDF by the software GCsolution; the raw LC-MS data (WIFF and SCAN files) were converted into mzXML files using

the software Proteo Wizard (http://proteowizard.sourceforge.net/). The converted files were imported to MZmine for filtering of retention time and *m/z* range, peak detection including mass detection, chromatogram build and peak deconvolution, alignment and peak finder functions. Retention time ranges of 11–55 min for GC-MS and 5–45 min for LC-MS were selected to avoid artifacts from derivatization agents and baseline noise, respectively. Peak detection was optimized to reduce the complexity of the chromatograms, avoid excessive noise features, and create a list of peaks that were each denoted by a specific mass and retention time. Peak alignment was done subsequently to adjust for slight variations in retention time and *m/z* values for different runs (Katajamaa and Orešič, 2005; Piletska et al., 2012). The parameters for Min time span, Min peak duration, *m/z* tolerance, retention time tolerance, and noise level were: (a) 0.1, 0.1, 0.2, 0.2 and 3 × 103 for GC-MS; (b) 0.1 0.1, 0.3, 0.3 and 1.5 × 105 for LC-MS negative mode; (c) 0.1, 0.1, 0.3, 0.5 and 5 × 105 for LC-MS positive mode, respectively. The deconvoluted and aligned datasets were exported to.csv files and normalized with EXCEL to reduce systematic error in the data comparisons.

Multivariate data analysis was performed with SIMCA-P+ version 13.0 (Umetrics, Umea, Sweden) for PCA and orthogonal partial least-squares discriminate analysis (OPLS-DA), which organized the observations, cultivar types, and variables according to their dependence on a small number of variables. The statistical results were visualized with a score plot that discriminated between the cultivars and among the wounding time points, establishing which values of *m/z* and retention time are responsible for these differences. As described previously (Dastmalchi et al., 2015; Wiklund, 2008), the OPLS-DA results were visualized in a scatter plot, in which the variables at the extreme ends (e.g., MS ions) were designated as potential biomarkers and verified as specific to a particular sample type using a variable line plot (Wiklund, 2008). The statistical model was validated by calculating values of R^2 and Q^2, indicators of fitness to the data and predictive ability, respectively (Worley and Powers, 2013). The value of Q^2, which is derived from cross validation of the model when a portion of the data is removed, was found to exceed 0.5 and the difference R^2-Q^2 was positive but small, as recommended (Wiklund, 2008).

5.9. Metabolite identification

GC-MS identification of compounds in the non-polar periderm extracts was accomplished by comparing the metabolite spectra with the National Institute of Standards and Technology (NIST) 2008 mass spectral library and Wiley Registry of Mass Spectral Data 9th library resident in the GCMSsolution software. Most of the metabolite identifications were based on the similarity score resulting from the comparison of our fragmentation patterns and the library data. Typically, spectral ions were assigned to a specific compound when the similarity score was higher than 80. The 2-monoacylglycerols were identified by comparing reported marked ions and EI fragmentation patterns, e.g., the fragments *m/z* 218, 203 and 191 that are characteristic for the β-isomer (Destaillats et al., 2010). As families of alkane compounds have similar MS patterns and fragments, a retention index (RI) was used to assist with identification by comparing their retention times against a standard C7–C40 saturated series (Sigma-Aldrich) with retention index values from 700 to 4000.

The metabolites of the polar extracts of native periderm were identified by comparing LC retention times and tandem MS/MS/MS fragments from the 4000 QTRAP analysis, and accurate masses from TOF-MS, with available literature reports. Searches were conducted using on-line databases such as Scifinder, Pubchem, and Metfrag to match the current data to a reported spectrum. Additionally, some metabolites for which no spectrum had been reported nevertheless displayed similar fragments to identified compounds, allowing for provisional assignment based on MS/MS fragmentation patterns and subsequent confirmation using TOF-MS data.

5.10. Wax compositional analyses by GC

The non-polar extracts were also used to determine the wax composition including the alkyl ferulates. The extracts were dried under nitrogen flow and derivatized using 20 µl of N,O-bis(trimethylsilyl)trifluoroacetamide (BSTFA; Macherey-Nagel) and 20 µl of pyridine (Sigma-Aldrich). The wax compositional data was obtained by GC-FID analysis performed using a Shimadzu GC-2010 Plus instrument using a BP1 capillary column (30 m length, 0.25 mm i.d., 0.1 µm film thickness, Teknokroma). A split/splitless injector in the splitless injection mode was used (splitless time 1 min) with the injector temperature at 280 °C and the detector temperature maintained at 320 °C. Helium was used as the carrier gas at a constant flow rate of 1 mL min^{-1}. Initially the oven temperature was at 120 °C, then increased by 20 °C min^{-1} up to 270 °C, then by 1.5 °C min^{-1} up to 340 °C and held at 340 °C for 7 min. Chromatograms were processed using GCSolution software (version 2.41) from Shimadzu. The percentage of each compound in the extract was calculated based on the individual integrated peak area divided by the sum of the areas of all identified compounds.

The compounds were identified in a GC-MS analysis using a GC Trace instrument (ThermoFisher) coupled to an ion trap mass spectrometer (PolarisQ, ThermoFisher), a BPX-5 capillary column (30 m length, 0.25 mm i.d., 0.25 µm film thickness) (SGE, Australia & Pacific Region) and helium as a carrier gas at 1 mL min^{-1}. A split/splitless injector in the splitless injection mode was used (splitless time 1 min) with the injector temperature at 280 °C. The oven temperature program was the same described for the GC-FID analyses. MS analyses were carried out with electron impact ionization operating at 70 eV and the ion source was set at 225 °C. The transfer line was held at 290 °C and acquisition was performed in full-scan mode, with a scan range of 50–700 amu. Chromatographic data were analyzed using Xcalibur 1.4 software.

5.11. Solid-state NMR analysis

The principal chemical moieties present in each of three dry biological replicate suberin extraction residues were determined using standard cross-polarization magic-angle spinning (CPMAS) ^{13}C NMR experiments carried out on a 4-channel Varian (Agilent) DirectDrive I (VNMRS) NMR 600 MHz spectrometer (Palo Alto, CA) equipped with a 1.6 mm HXY FastMAS probe. The ^{13}C resonance frequency was 150.757,400 MHz, with a customary acquisition time of 25 ms, a delay time of 3 s between successive acquisitions, a CP contact time of 1.5 ms, and a 200 kHz ^{1}H decoupling strength achieved using the SPINAL method (Fung et al., 2000). Typically, 5 mg samples were spun at 10,000 ± 20 Hz for approximately 7 h. The resulting CPMAS data were processed using VNMRJ (version 2.2C; Agilent) and/or ACD/NMR Processor Academic Edition 12 (Advanced Chemistry Development, Inc., Toronto, ON, Canada) with 100 Hz of exponential line broadening to improve the signal-to-noise ratio of the spectra. Chemical shift referencing was done externally using the methylene ($-CH_2-$) group of adamantane (Sigma-Aldrich) set to 38.48 ppm.

To estimate ratios of the various carbon types, quantitatively reliable direct-polarization magic-angle-spinning (DPMAS) ^{13}C NMR spectra of these amorphous plant materials (Serra et al., 2014; Zlotnik-Mazori and Stark, 1988) were acquired with 3000 scans for 83 h. A customary acquisition time of 25 ms and delay time of 100 s

between successive acquisitions were used. After applying exponential line broadening of 200 Hz, signal intensities in the DPMAS spectra were measured by cut-and-weigh-paper methods and by counting pixels using Photoshop software for the following regions: carboxyl groups (COO; 160–180 ppm), multiply bonded groups (aromatics and alkenes; 92–160 ppm), oxygenated aliphatic carbon groups ($CHO + CH_2O + CH_3O$; 44–92 ppm) and long-chain methylene groups ($-(CH_2)_n-$; 10–44 ppm). Ratios of integrated signal intensities for particular spectral regions were measured for each cultivar using both methods; error bars represent the difference between the two values.

5.12. Thioacidolysis analysis

Between 10 and 45 mg of native potato tuber periderm samples previously treated with 2% of cellulase and pectinase as described (Serra et al., 2010) were used as starting tissue for each replicate. Prior to thioacidolysis analysis the samples were treated with methanol:chloroform (1:1, v/v) overnight to remove the extractives and with methanol/boron trifluoride (~10% BF_3 in methanol; Fluka) overnight to remove the aliphatic suberin polyester as described in Serra et al. (2010). The remaining insoluble residue was subjected to thioacydolysis to determine the lignin-like composition by GC–FID of lignin-derived monomer trimethylsilyl derivatives (Lapierre et al., 1986). H, G and S units were identified by comparison with commercially available standards. The amount of each unit was related to the weight of the dried starting material.

Acknowledgements

The authors thank Dr. Hsin Wang, Dr. Lijia Yang, Ms. Cristina Veresmortean, and Mr. Boris Kalmatsky for valuable technical assistance with the NMR, LC-MS/MS, LC-TOF, and GC-MS instrumentation at The City College of New York. We also thank Dr. Enriqueta Anticó for technical assistance with the wax GC compositional analyses. This work was supported by grants from the U.S. National Science Foundation (NSF MCB-0843627, 1411984, and 0741914 to R.E.S.), from the Spanish Ministerio de Economía y Competitividad and FEDER funding (AGL2012-36725; AGL2015-67495-C2-1-R), and from the University of Guelph (MPCUdG2016/078). The NMR resources were operated by The City College of New York and the CUNY Institute for Macromolecular Assemblies. Infrastructural support for the NMR facilities was provided by the U.S. National Institutes of Health (5G12MD007603-30 from the National Institute on Minority Health and Health Disparities). The GC-MS instrument was supported by the U.S. NSF (CHE-0840498) and the GC-FID instrument by the University of Guelph (SING11/1).

Appendix A. Supplementary data

Supplementary data related to this article can be found at https://doi.org/10.1016/j.phytochem.2017.12.011.

References

Akyol, H., Riciputi, Y., Capanoglu, E., Carboni, M.F., Verado, V., 2016. Phenolic compounds in the potato and its byproducts: an overview. Int. J. Mol. Sci. 17, 835.

Bassard, J.-E., Ulmann, P., Bernier, F., Wreck-Reichhart, D., 2010. Phenolamides: bridging polyamine to the phenolic metabolism. Phytochemistry 71, 1808–1824.

Bernard, A., Domergue, F., Pascal, S., Jetter, R., Renne, C., Faure, J.-D., Haslam, R.P., Napier, J.A., Lessire, R., Joubes, J., 2012. Reconstitution of plant alkane biosynthesis in yeast demonstrates that *Arabidopsis* ECERIFERUM1 and ECERIFERUM3 are core components of a very-long-chain alkane synthesis complex. Plant Cell 24, 3106–3118.

Bernards, M.A., 2002. Demystifiying suberin. Can. J. Bot. 80, 227–240.

Boher, P., Serra, O., Soler, M., Molinas, M., Figueras, M., 2013. The potato suberin feruloyl transferase FHT which accumulates in the phellogen is induced by wounding and regulated by abscisic and salicylic acids. J. Exp. Bot. 64 (11), 3225–3236.

Choi, H.-K., Choi, Y.H., Verberne, M., Lefeber, A.W.M., Erkelens, C., Verpoorte, R., 2004. Metabolic fingerprinting of wild type and transgenic tobacco plants by ^1H NMR and multivariate analysis technique. Phytochemistry 65, 857–864.

Dastmalchi, K., Cai, Q., Zhou, K., Huang, W., Serra, O., Stark, R.E., 2014. Completing the jigsaw puzzle of wound-healing potato cultivars: metabolite profiling and antioxidant activity of polar extracts. J. Agric. Food Chem. 62, 7963–7975.

Dastmalchi, K., Kallash, L., Wang, I., Phan, V.C., Huang, W., Serra, O., Stark, R.E., 2015. Defensive armor of potato tubers: non-polar metabolite profiling, antioxidant assessment, and solid-state NMR compositional analysis of suberin-enriched wound-healing tissues. J. Agric. Food Chem. 63, 6810–6822 .

Dawid, C., Hofmann, T., 2014. Quantitation and bitter taste contribution of saponins in fresh and cooked white asparagus (*Asparagus officinalis* L.). Food Chem. 145, 427–436.

Dean, B.B., Kolattukudy, P.E., 1976. Synthesis of suberin during wound-healing in jade leaves, tomato fruit, and bean pods. Plant Physiol. 58, 411–416.

Destaillats, F., Cruz-Hernandez, C., Nagy, K., Dionisi, F., 2010. Identification of monoacylglycerol regioisomers by gas chromatography-mass spectrometery. J. Chromatogr. A A1217, 1543–1548.

Duo, J., Zang, Y., Yu, G., Zhao, S., Song, Q., 2007. Interannual and seasonal variations of energy and water vapor fluxes above a tropical seasonal rain forest in Xishuangbanna, SW China. Acta Ecol. Sinica 27, 3099–3109.

FAO, 2015. FAO Statistical Pocketbook: World Food and Agriculture. Food and Agriculture Organization of the United Nations.

Franke, R., Briesen, I., Wojciechowski, T., Faust, A., Yephremov, A., Nawrath, C., Schreiber, L., 2005. Apoplastic polyesters in *Arabidopsis* surface tissues–a typical suberin and a particular cutin. Phytochemistry 66, 2643–2658.

Fraser, C.M., Chapple, C., 2011. The phenylpropanoid pathway in arabidopsis. In: The Arabidopsis Book, vol. 9. The American Society of Plant Biologists, p. e0152.

Fung, B.M., Khitrin, A.K., Ermolaev, K., 2000. An improved broadband decoupling sequance for liquid crystals and solids. J. Magn. Reson. 142, 97–101.

Garbow, J.R., Ferrantello, L.M., Stark, R.E., 1989. ^{13}C nuclear magnetic resonance study of suberized potato cell wall. Plant Physiol. 90, 783–787.

Ginzberg, I., Minz, D., Faingold, I., Soriano, S., Mints, M., Fogelman, E., Warshavsky, S., Zig, U., Yermiyahu, U., 2012. Calcium mitigated potato skin physiological disorder. Am. J. Potato Res. 89 (5), 351–362.

Gil, A.M., Lopes, M., Rocha, J., Neto, C.P.A., 1997. ^{13}C solid state nuclear magnetic resonance spectroscopic study of cork cell wall structure: the effect of suberin removal. Int. J. Biol. Macromol. 20, 293–305.

Graça, J., 2015. Suberin: the biopolyester at the frontier of plants. Front. Chem. 3, 62.

Graça, J., Pereira, H., 2000. Suberin structure in potato periderm: glycerol, long-chain monomors, and glycerol and feruloyl dimers. J. Agric. Food Chem. 48, 5476–5483.

Graça, J., Santos, S., 2007. Suberin: a biopolyester of plants' skin. Macromol. Biosci. 7, 128–135.

Hammes, K., Smernik, R.J., Skjemstad, J.O., Herzog, A., Vogt, U.F., Schmidt, M.W.I., 2006. Synthesis and characterisation of laboratory-charred grass straw (*Oryza sativa*) and chestnut wood (*Castanea sativa*) as reference materials for black carbon quantification. Org. Geochem. 37, 1629–1633.

Heng, W., Wang, Z., Jiang, X., Jia, B., Liu, P., Liu, L., Ye, Z., Zhu, L., 2016. The role of polyamines during exocarp formation in a russeted mutant of 'Dangshansuli' pear (*Pyrus bretschneideri* Rehd.). Plant Cell Rep. 35, 1841–1852.

Huang, W., Serra, O., Dastmalchi, K., Liqing, J., Yang, L., Stark, R.E., 2017. Comprehensive MS and Solid-State NMR metabolite profiling reveals molecular variations in native periderms from four *Solanum tuberosum* potato cultivars. J. Agric. Food Chem. 65, 2258–2274.

Järvinen, R., Silvestre, A.J.D., Gill, A.M., Kallio, H., 2011. Solid state ^{13}C CP-MAS NMR and FT-IR spectroscopic analysis of cuticular fractions of berries and suberized membranes of potato. J. Food Compos. Anal. 24, 334–345.

Katajamaa, M., Miettinen, J., Orešič, M., 2006. MZmine: toolbox for processing and visualization of mass spectrometry based molecular profile data. Bioinformatics 22, 634–636.

Katajamaa, M., Orešič, M., 2005. Processing methods for differential analysis of LC/MS profile data. BMC Bioinf. 6, 179.

Kim, H.K., Choi, Y.H., Verpoorte, R., 2010. NMR-based metabolomic analysis of plants. Nat. Protoc. 5, 536–549.

King, R.R., Calhoun, L.A., 2005. Characterization of cross-linked hydroxycinnamic acid amides isolated from potato common scab lesions. Phytochemistry 66, 2468–2473.

King, R.R., Calhoun, L.A., 2010. A feruloyltyrmaine trimer isolated from potato common scab lesions. Phytochemistry 71, 2187–2189.

Landgraf, R., Smolka, U., Altmann, S., Eschen-Lippold, L., Senning, M., Sonnewald, S., Weigel, B., Frolova, N., Strehmel, N., Hause, G., Scheel, D., Bottcher, C., Rosahl, S., 2014. The ABS transporter ABGCG1 is required for suberin formation in potato tuber periderm. Plant Cell 26, 3403–3415.

Lapierre, C., Pollet, B., Négrel, J., 1996. The phenolic domain of potato suberin: structural comparison with lignins. Phytochemistry 42 (4), 949–953.

Lapierre, C., Pollet, B., Rolando, C., 1995. New insights into the molecular architecture of hardwood lignins by chemical degradative methods. Res. Chem. Intermed. 21, 397–412.

Lapierre, C., Rolando, C., Monties, B., 1986. Thioacidolysis of poplar lignins: identification of monomeric syringyl products and characterization of guaiacyl syringylfractions. Holzforschung 40, 113–118.
Lulai, E.C., Campbell, L.G., Fugate, K.K., McCue, K.F., 2016. Biological differences that distinguish the 2 major stages of wound healing in potato tubers. Plant Signal. Behav. 11 (12), e31256531.
Lulai, E.C., Corsini, D.L., 1998. Differential deposition of suberin phenolic and aliphatic domains and their roles in resistance to infection during potato tuber (*Solanum tuberosum* L.) wound-healing. Physiology and Molecular Plant Biology 53, 209–222.
Lulai, E.C., Neubauer, J.D., 2014. Wound induced suberization genes are differentially expressed during closing layer and wound periderm formation. Am. J. Potato Res. 91, 54.
Lulai, E.C., Orr, P.H., 1994. Techniques for detecting and measuring developmental and maturational changes in tuber native periderm. Am. J. Potato Res. 71, 489–505.
Martin-Tanguy, J., 1985. The occurrence and possible function of hydroxycinnamoyl acid amides in plants. Plant Growth Regul. 3, 381–399.
Matsuda, F., Morino, K., Ano, R., Kuzawa, M., Wakasa, K., Miyagawa, H., 2005. Metabolic flux analysis of the phenylpropanoid pathway in elicitor-treated potato tuber tissue. Plant Cell Physiol. 46 (3), 454–466.
Narvaez-Cuenca, C.-E., Vincken, J.-P., Gruppen, H., 2012. Identification and quantification of (dihydro) hydroxycinnamic acid and their conjugates in potato by UHPLC-DAD-ESI-MS^n. Food Chem. 130, 730–738.
Négrel, J., Pollet, B., Lapierre, C., 1996. Ether-linked ferulic acid amides in natual and wound periderms of potato tubers. Phytochemistry 43 (6), 1195–1199.
Neubauer, J.D., Lulai, E.C., Thompson, A.L., Suttle, J.C., Bolton, M.D., 2012. Wounding coordinately induces cell wall protein, cell cycle and pectin methyl esterase genes involved in tuber closing layer and wound periderm development. J. Plant Physiol. 169, 586–595.
Pacchiano Jr., R.A., Sohn, W., Chlanda, V.L., Garbow, J.R., Stark, R.E., 1993. Isolation and spectral characterization of plant-cuticle polyesters. J. Agric. Food Chem. 41, 78–83.
Pascoal Neto, C., Rocha, J., Gil, A., Cordeiro, N., Esculcas, A.P., Rocha, J., Delgadillo, I., de Jesus, J.D., Corriera, A.J.F., 1995. ^{13}C solid-state nuclear magnetic resonance and Fourier transform infrared studies of the thermal decomposition of cork. Solid State Nucl. Magn. Reson. 4, 143–151.
Piletska, E.V., Burns, R., Terry, L.A., Piletsky, S.A., 2012. Application of a molecularly imprinted polymer for the extraction of kukoamine a from potato peels. J. Agric. Food Chem. 60, 95–99.
Pluskal, T., Castillo, S., Villar-Briones, A., Oresic, M., 2010. MZmine 2: modular framework for processing, visualizing and analyzing mass spectrometry-based molecular profile data. BMC Bioinf. 11, 395.
Sabba, R.P., Lulai, E.C., 2002. Histological analysis of the maturation of native and wound periderm in potato (*Solanum tuberosum* L.) tuber. Ann. Bot. 90, 1–10.
Schreiber, L., Franke, R., Hartmann, K., 2005. Wax and suberin development of native and wound periderm of potato (*Solanum tuberosum* L.) and its relation to peridermal transpiration. Planta 220, 520–530.
Serra, O., Chatterjee, S., Figueras, M., Molinas, M., Stark, R.E., 2014. Deconstructing a plant macromolecular assembly: chemical architecture, molecular flexibility, and mechanical performance of natural and engineered potato suberins. Biomacromolecules 15, 799–811.
Serra, O., Hohn, C., Franke, R., Prat, S., Molinas, M., Figueras, M., 2010. A feruloyl transferase involved in the biosynthesis of suberin and suberin-associated wax is required for maturation and sealing properties of potato periderm, 62, 277–290.
Shakya, R., Navarre, D.A., 2008. LC-MS analysis of solanidane glycoalkaloid diversity among tubers of four wild potato species and three cultivars (*Solanum tuberosum*). J. Agric. Food Chem. 56, 6949–6958.
Stark, R.E., Sohn, W., Pacchiano Jr., R.A., Al-Bashir, M., Garbow, J.R., 1994. Following suberization in potato wound periderm by histochemical and solid state ^{13}C nuclear magnetic resonance methods. Plant Physiol. 104, 527–533.
Volpert, R., Osswald, W., Elstner, E.F., 1995. Effects of cinnamic acid derivatives on indole acetic acid oxidation by peroxidase. Phytochemistry 38, 19–22.
Want, E., Masson, P., 2011. Processing and analysis of GC/LC-MS-based metabolomics data. Meth. Mol. Biol. 708, 277–298.
Wiklund, J.R., 2008. Multivariate data analysis and modelling in “omics.” In: Umetrics, S.J. (Ed.), AB, CA.
Wolfram, W., 2006. Metabolomics: Methods and Protocols, first ed.
Worley, B., Powers, R., 2013. Multivariate analysis in metabolomics. Current Metabolomics 1, 92–107.
Yang, W., Pollard, M., Li-Beisson, Y., Beisson, F., Feig, M., Ohlrogge, J., 2010. A disitnict type of glycerol-3-phosphate acyltransferase with *sn*-2 preference and phosphates activity producing 2-monoacylglycerol. Proc. Natl. Acad. Sci. U.S.A. 107, 12040–12045.
Yang, W.L., Bernards, M.A., 2006. Wound induced metabolism in potato (*Solanum tuberosum*) tubers: biosynthesis of aliphatic domain monomors. Plant Signal. Behav. 1, 59–66.
Yang, W.L., Bernards, M.A., 2007. Metabolite profiling of potato (*Solanum tuberosum* L.) tubers during wound-induced suberization. Metabolomics 3, 147–159.
Zlotnik-Mazori, T., Stark, R.E., 1988. Nuclear magnetic reosnance studies of cutin, an insoluble plant polyester. Macromolecules 21, 2412–2417.